Local endoreduplication as a feature of intracellular fungal accommodation in arbuscular mycorrhizas

New Phytologist

Local endoreduplication as a feature of intracellular fungal accommodation in arbuscular mycorrhizas

Journal:	*New Phytologist*
Manuscript ID	NPH-MS-2018-28499.R1
Manuscript Type:	MS - Regular Manuscript
Date Submitted by the Author:	n/a
Complete List of Authors:	Carotenuto, Gennaro; Università di Torino, Dipartimento di Scienze della Vita e Biologia dei Sistemi Volpe, Veronica; Università degli Studi di Torino, Department of Life Science and Systems Biology Russo, Giulia; Università di Torino, Dipartimento di Scienze della Vita e Biologia dei Sistemi ; Michigan State University, Politi, Mara; Università di Torino, Dipartimento di Scienze della Vita e Biologia dei Sistemi Sciascia, Ivan; Università di Torino, Dipartimento di Scienze della Vita e Biologia dei Sistemi de Almeida Engler, Janice; INRA PACA Site de Sophia-Antipolis, CNRS, ISA, 06903 Genre, Andrea; Università di Torino, Dipartimento di Scienze della Vita e Biologia dei Sistemi
Key Words:	endoreduplication, ploidy, arbuscular mycorrizas, Medicago truncatula, Gigaspora margarita, flow cytometry, Confocal imaging, Symbiosis

Title page

Authors

Gennaro Carotenuto[1], Veronica Volpe[1], Giulia Russo[1], Mara Politi[1], Ivan Sciascia[1], Janice de Almeida-Engler[2], Andrea Genre[1]

[1]Department of Life Sciences and Systems Biology, University of Turin, 10125 Torin, Italy; [2]INRA, Université Côte d'Azur, CNRS, ISA, 06903, Sophia Antipolis, France

Corresponding author:

Andrea Genre: andrea.genre@unito.it, Tel: +39 011 6705083

Title

Local endoreduplication as a feature of intracellular fungal accommodation in arbuscular mycorrhizas

Short title

Local endoreduplication in arbuscular mycorrhizas

Total word count for the main body:	6410
Word count for section Introduction:	863
Word count for Materials and methods:	1389
Word count for Results:	2651
Number of Figures:	9
Number of colored Figures:	7
Number of Supplementary Figures:	7
Number of tables:	0
Word count for Discussion:	1378

ORCID

Gennaro Carotenuto https://orcid.org/0000-0001-8338-9952
Janice deAlmeida-Engler https://orcid.org/0000-0002-8312-672X
Andrea Genre http://orcid.org/0000-0001-7768-3047
Giulia Russo http://orcid.org/0000-0003-4762-3777
Ivan Sciascia https://orcid.org/0000-0001-9012-4987
Veronica Volpe http://orcid.org/0000-0002-3559-7615

SUMMARY

• The intracellular accommodation of arbuscular mycorrhizal (AM) fungi is a paradigmatic feature of this plant symbiosis that depends on the activation of a dedicated signaling pathway and the extensive reprogramming of host cells, including striking changes in nuclear size and transcriptional activity.

• By combining targeted sampling of early root colonization sites, detailed confocal imaging, flow cytometry and gene expression analyses, we demonstrate that local, recursive events of endoreduplication are triggered in the *Medicago truncatula* root cortex during AM colonization.

• AM colonization induces an increase in ploidy levels and the activation of endocycle specific markers.

• This response anticipates the progression of fungal colonization and is limited to arbusculated and neighboring cells in the cortical tissue.

• Furthermore, endoreduplication is not induced in *M. truncatula* mutants for symbiotic signaling pathway genes.

• On this basis, we propose endoreduplication as part of the host cell prepenetration responses that anticipate AM fungal accommodation in the root cortex.

INTRODUCTION

Glomeromycotina form a widespread group of soil-born fungi (Spatafora *et al*., 2016) that establish mutualistic arbuscular mycorrhizal (AM) symbiosis with most land plants, including the majority of crop species (Smith & Read, 1997; Salvioli & Bonfante, 2013). Soil exploration by the root-associated mycelium provides the host plant with privileged access to water and mineral nutrients such as phosphorus and nitrogen (Gutjahr & Parniske 2013). In return, host plants feed their symbionts with carbon compounds (McLean *et al*., 2017). Root colonization by AM fungi is limited to epidermal and cortical tissues. It initiates with the formation of a hyphopodium on the root epidermis, followed by hyphal penetration in single epidermal cells and subsequent proliferation of inter- and intracellular hyphae in the root cortex. Arbuscules develop from the repeated branching of intracellular hyphae in the inner cortex and are considered the main site of nutrient exchange (Gutjahr & Parniske, 2013). Due to its ancient evolutionary origin, AM symbiosis is hypothesized to have several features that were co-opted for symbiotic nitrogen fixation (SNF) in legumes (Parniske, 2008). These include the activation of a set of proteins that constitute the common symbiotic signaling pathway (CSSP) (Oldroyd 2013), and the generation and decoding of nuclear calcium oscillations in response to both AM fungal and rhizobial elicitors (Gutjahr & Parniske, 2013). In addition, AM hyphae enter plant cells via an intracellular accommodation structure, called the prepenetration apparatus or PPA (Genre *et al*., 2005; 2008), which shares several similarities with SNF pre-infection thread (Gage, 2004) and drives intracellular hyphal development.

In fact, the accommodation of hyphae and arbuscules requires a profound reprogramming of host cell architecture (Dörmann *et al*., 2014). These comprise nuclear movements, vacuole partitioning, cytoskeletal rearrangement and the formation of cytoplasmic bridges (PPA) in coordination with fungal development (Gutjahr & Parniske, 2013). Host cell reprogramming is particularly extensive in arbuscule-containing cells, with major cytological modifications and changes in gene expression that also extend to neighboring cortical cells (Blancaflor *et al*., 2001; Genre *et al*., 2008; Pumplin & Harrison, 2009; Gaude *et al*., 2012).

We have recently demonstrated that arbuscule accommodation involves the reactivation of the cell cycle in the root cortex (Russo *et al*., 2019), where ectopic cell division generates spread couples of so-called split cells in advance of arbuscule development. Furthermore, PPA-associated expression and recruitment of exocytic cell plate markers, such as TPLATE, suggest that the cell plate assembly machinery is rerouted towards the biogenesis of the periarbuscular interface in the absence of cell

division. On this basis we hypothesized that cell cycle activation without mitosis in arbusculated cells should lead to an increase in ploidy through endoreduplication. To test this hypothesis, we therefore investigated if fungal accommodation is associated with local ploidy changes.

Indirect support for this hypothesis comes from previous studies reporting increased nuclear size in arbusculated cells of several angiosperms (Balestrini *et al*. 1992, Fusconi *et al*. 2005, Genre *et al*. 2008, Bainard *et al*. 2011, Ivanov & Harrison 2014) alongside with chromatin decondensation, another hallmark of endoreduplication (Berta *et al*., 2000; Repetto *et al*., 2007; Bainard *et al*., 2011). Nevertheless, limited evidence is available of a correlation in time and space between nuclear changes and the progression of fungal colonization, leaving the molecular mechanisms of host cell cycle manipulation by mycorrhizal fungi largely unexplored.

Endoreduplication - also known as endocycle - is a specialized cell cycle in which cells undergo S phase but do not divide, resulting in the generation of polyploid cells with multiple DNA duplication events (Kondorosi *et al*., 2000). Cell cycle reactivation is a widespread feature in developmental programs of most seed plants, including the model legume *Medicago truncatula* (Barrow & Meister, 2003; Kondorosi & Kondorosi, 2004), as well as in responses to abiotic (Van Oostveldt *et al*., 1975; Galli, 1988; Cavallini *et al*., 1995; Engelen-Eigles *et al*., 2000) and biotic stimuli (Barrow, 2006; Wildermuth *et al*., 2010). Endocycle is typically activated during differentiation of several cell types with specialized functions (Kondorosi & Kondorosi, 2004) and results in polysomaty, a condition where cells with different ploidy levels are found next to each other (Smulders *et al*., 1994).

The switch from mitosis to endocycle is finely regulated through targeted proteolysis, transcriptional repression or post-translational inhibition of cyclin dependent kinases (CDK) and mitotic cyclins (De Veylder *et al*., 2007; 2011). In higher plants, the best studied mechanism of endocycle regulation involves the ubiquitin-proteasome degradation of mitotic CDK by APC/C, the Anaphase-Promoting Complex (Harper *et al*., 2002; Buschhorn & Peters, 2006). An alternative molecular trigger is the transcriptional down-regulation of CDK and G2-M-expressed genes by the transcription factor Increased Level of Polyploidy 1 (ILP1; Yoshizumi *et al*., 2006).

Our present results indicate that endoreduplication events are activated in root cortical cells of wild-type *Medicago truncatula* inoculated with the AM fungus *Gigaspora margarita*, but not in *dmi2-2* and *dmi3-1* CSSP mutants. Combined flow cytometry and confocal microscopy imaging localize the occurrence of endoreduplication in colonized and surrounding cells of the root cortex, suggesting that ploidy increase is associated with fungal accommodation and prepenetration responses. In addition, endocycle and S-phase markers were significantly upregulated in colonized root segments,

altogether providing sound support to our conclusion that endocycle activation is a symbiotic feature of AM interactions.

MATERIALS AND METHODS

Plant materials

All experiments were performed using *Medicago truncatula* plants (genotype Jemalong A17) and explants of three *Agrobacterium rhizogenes*–generated root organ cultures (ROCs) lines: one derived from the same wild-type *M. truncatula* cultivar and two from CSSP mutants *dmi2-2* and *dmi3-1*, (Catoira *et al*., 2000; Morandi *et al*., 2005). ROC lines, already available in the lab (Chabaud *et al*., 2011; Genre *et al*., 2013), expressed a nuclear localized cameleon YC2.1 construct, and were propagated on M medium (Bécard & Fortin, 1988) at 25°C in the dark, in vertically oriented petri dishes to favour a regular fishbone-shaped root system (Chabaud *et al*., 2002). Explants with consistent morphology and an identical number of lateral roots were chosen for all ROC-based experiments (Russo *et al*., 2019).

Fungal materials

The AM fungus *Gigaspora margarita* isolate BEG34 (International Bank for the Glomeromycota, University of Kent, Canterbury, UK) was chosen for its amenability to both pot and *in vitro* experiments. Fungal spores were collected from pot cultures of mycorrhizal *Trifolium repens*, vernalized at 4°C for 2 weeks, and surface sterilized with 3% (w/v) chloramine T and 0.03% (w/v) streptomycin, according to Lanfranco *et al*. (2005).

Arbuscular mycorrhizal colonization of wild-type *Medicago truncatula* plants

Wild-type *M. truncatula* seeds were germinated on water agar (0.6%) in Petri dishes as described in Russo *et al*. (2019). Seven-day-old seedlings were inoculated with sterilized *G. margarita* spores using the Millipore sandwich method (Giovannetti *et al*., 1993). Briefly, seedlings were placed between two nitrocellulose membranes with twenty *G. margarita* spores. Inoculation was omitted in controls. Uninoculated and inoculated sandwiches were planted in sterile quartz sand, watered with Long-Ashton solution containing 3.2 µM $Na_2HPO_4 \cdot 12H_2O$ and 0.5 mM $NaNO_3$ (Hewitt, 1966) and grown in a climatic chamber with a 14 h light (24°C)/10 h dark (20°C) photoperiod. After 35

days, 1 cm-long samples of colonized roots – bound to abundant extraradical mycelium – and uninoculated root samples of comparable age and size were excised using a stereo microscope and processed for confocal imaging and flow cytometry. Two independent experiments and a total of 15 uninoculated and 15 inoculated plants were analysed.

Targeted inoculation of root organ culures

The targeted AM inoculation technique (Chabaud *et al*., 2002) was chosen to take advantage of direct observation of colonization events and collection of early colonized samples and adjacent zones. In short, two growing explants of wild-type, *dmi2-2* and *dmi3-1 M. truncatula* ROCs (Chabaud *et al*., 2011; Genre *et al*., 2013) were inoculated with four pre-germinated spores of *G. margarita* in each Petri dish. Fungal growth and root colonization were monitored daily under a stereo microscope to identify hyphopodium development. Cameleon YC2.1 yellow fluorescence was used to check for nuclear repositioning in epidermal cells under the hyphopodia, a hallmark of early prepenetration responses. One cm-long sub-hyphopodial root segments were harvested 48/60 hours after hyphopodium formation and all meristems were removed using a scalpel. Each biological replicate used for confocal imaging, flow cytometry or gene expression analyses included a pool of at least 15 segments, deriving from at least 3 independent ROCs.

Nuclear staining and confocal imaging

Uninoculated and inoculated samples from sandwich or ROC cultures were fixed and sectioned longitudinally in 100µm-thick sections using a Vibratome (Oxford Vibratome®), as described by Vieira *et al.* (2012), with minor modifications (Supplementary Method S1).

Imaging was performed with an upright Leica TCS SP2 confocal microscope fitted with a long distance 40X water-immersion objective (HCX Apo 0.80), using the 405 nm diode for DAPI excitation. To better visualize intraradical fungal hyphae, selected samples were stained overnight at room temperature with acid fuchsin (Kormanik & McGraw, 1982) and imaged using 488nm excitation and 600-700nm emission filters. Alternatively, DAPI-stained sections were washed three times in PBS and counterstained for 10 min at RT (Musielak *et al*., 2016) with 0.1% SCRI Renaissance 2200 (SR2200; Renaissance Chemicals Ltd, North Duffield, Selby, UK) in PBS supplemented with 1% DMSO, 0.05% TritonX-100, 5% glycerol and 3.75% paraformaldehyde). Following a 10 min rinse in PBS, sections were mounted in 90% glycerol and imaged using the 405 nm diode for excitation of

both fluorochromes. Confocal images were false-coloured in green for DAPI and yellow for acid fuchsin and SR2200.

Nuclear area and volume measurements

Nuclear areas and volumes were analyzed in z-stacks of 375x375x45µm (1.5µm z step) derived from at least 25 independent sections (and five independent roots) per experimental condition, as described in Supplementary Methods S2. Maximum brightness projections of z-stacks are presented in the figures.

Data analysis

Following the collection of nuclear area measurements from wild-type, *dmi2-2* and *dmi3-1* ROC lines, we applied Sturges' rule (Sturges, 1926), a statistical method that distributes data into an optimal number of classes based on population characteristics, including the average sample size (160 measurements per section in our case). Sturges' rule divided our data into 8 classes for wild-type mycorrhizal roots (with a class amplitude of 15 μm^2) and 7 classes (with an amplitude of 13 μm^2) for both *dmi2-2* and *dmi3-1* mutants (average sample of 110 measures per section).

Pearson's correlation coefficient and Fisher's test were calculated to test the correlation among mean area values for each Sturges class and ploidy levels. Logarithmic regression models were fitted to the data to represent the relationship between nuclear areas and ploidy levels (Supplemental Figure S7).

The class subdivisions were used to label the measured nuclei on maximum brightness projection images, developing an atlas of nuclear sizes for wild-type, *dmi2*-2 and *dmi3-1* for each experimental condition.

Flow cytometry analysis of ploidy

The analysis of nuclear DNA content by flow cytometry was performed as described by Vieira *et al*. (2013). Extracted nuclei were analysed using an LSRII Fortessa (BD Biosciences) flow cytometer and the BD FACS Diva Software (BD Biosciences). Since the intrinsic fluorescence of the nuclear-localized NupYC2.1 probe was not sufficient to identify ploidy classes in flow cytometry, we stained DNA with propidium iodide.

Approximately 30000 and 25000 nuclei per run were analysed for uninoculated and inoculated samples, respectively. In each independent experiment, at least fifteen 1cm-long root samples

belonging to 5 independent ROCs were pooled in four technical replicates, and the average percent value of each ploidy class was calculated. Three experiments were run for wild-type ROCs, two for each CSSP-mutant ROC line, and the averages are presented in Figures 3, 4 and 6. All statistical analyses were done using Past multivariate statistics package v3.0 (Hammer *et al*., 2004). The statistical differences in the percentages of endoreduplicated nuclei (> 8C) between uninoculated and inoculated root segments were evaluated with Chi-Square test ($P < 0.01$).

RNA extraction, cDNA synthesis and RT-PCR

Four uninoculated and four inoculated biological replicates were collected from wild-type, *dmi2*-2 and *dmi3-1* ROCs to investigate gene expression. Each biological replicate consisted of fifteen 1cm-long root segments harvested from at least five independent ROCs and were sampled 48/60 hours after hyphopodium formation. Samples were rapidly deprived of all visible root meristems and immediately flash-frozen in liquid nitrogen.

RNA extraction and gene expression analyses were performed according to Russo *et al*. (2019), using a TissueLyser system (Qiagen, Hilden, Germany) for sample disruption, RNeasy™ Plant Mini kit (Qiagen, Hilden, Germany) for RNA extraction and TURBO™ DNase (Ambion, Austin, TX) to remove DNA contamination. Purified RNA samples were checked for DNA contamination by PCR analysis, using *MtTEF* (*Elongation Factor 1α*) primers (Supporting information Table S1).

Specific primers for *MtBCBP*, *MtPUB1*, *MtILP1*, *MtAPC/C subunit 2*, *MtCCS52A*, *MtTOPO-VI A*, *MtTopo-VI B*, *MtHist-H4* and *MtE2Fe-DEL1* were designed based on *M. truncatula* CDS sequences from NCBI database (http://www.ncbi.nlm.nih.gov/) using SerialCloner software (Supporting Information Table S1). Primer validation was performed by conventional PCR assays on *M. truncatula* cDNA and *G. margarita* genomic DNA to exclude the detection of non-specific sequences. Quantitative RT-PCR analyses were done with a Rotor Gene 6000 machine (Qiagen, Hilden, Germany) as described in Russo et al. (2019). All reactions were performed with three technical replicates. The comparative threshold cycle method (Rasmussen, 2001) was used to calculate calibrated normalized relative quantities (CNRQ) of gene expression based on gene specific amplification efficiencies using the plant *MtTEF* (Hohnjec *et al*., 2005) as a reference gene. Prior to statistical analysis, CNRQ values were log-transformed.

246 **Accession numbers**

247 Sequence data from this article can be found in the EMBL/GenBank data libraries under the
248 following accession numbers: MTR_1g105120 (*MtBCBP*); Medtr5g090510 (*MtPUB1*);
249 MTR_5g007520 (*MtILP1*); MTR_4g082150 (*MtAPC/C subunit 2*); MTR_4g102510 (*MtCCS52A*);
250 MTR_6g077860 (*MtTOPO-VI A*); MTR_2g098510 (*MtTOPO-VI B*); MTR_7g029520 (*MtHist-H4*
251 partial); MTR_4g106540 (*MtE2Fe-DEL1*) and MTR_6g021805 (*MtTEF*).

252

253 **RESULTS**

254

255 **AM colonization associates with nuclear size increase in both whole plants and ROCs**

256 Confocal microscopy observations of 100μm-thick sections from DAPI-stained mycorrhizal root
257 segments of wild-type *M. truncatula* plants revealed obvious changes in nuclear size and shape in
258 arbusculated cells compared to cortical cells from uninoculated roots (Fig. 1). Based on this
259 observation, we measured the size of all visible nuclei in longitudinal root sections. Our analysis (Fig.
260 1e) confirmed that the average nuclear area in mycorrhizal root sections (32.4 ± 0.3 μm^2) was
261 significantly increased by ~1.4 fold compared to uninoculated roots (23.4 ± 0.1 μm^2). Furthermore,
262 frequency distributions of nuclear areas (Fig. S1a) were significantly larger (Kruskal-Wallis test at P
263 < 0.01) in mycorrhizal roots (ranging between 15 to 111 μm^2) than controls (15 to 43 μm^2).
264 Using the Fiji plugin 3D-Object Counter to measure nuclear volumes in the same confocal z-stacks
265 (Figure 1f) confirmed the increase in average nuclear volume for mycorrhizal (49 ± 1.4 μm^3)
266 compared to uninoculated root sections (35.3 ± 0.6 μm^3). Also in this case, the frequency
267 distribution of nuclear volumes (Fig. S1b; Kruskal-Wallis test at P < 0.01) was larger in mycorrhizal
268 (20 to 205 μm^3) than in uninoculated roots (20 to 119 μm^3).
269 Our combined 2D and 3D measurement of nuclear size suggested a significant increase in
270 mycorrhizal compared to uninoculated *M. truncatula* roots, with the appearance of a dispersed
271 population of enlarged nuclei in the presence of AM colonization. These results extended previous
272 descriptions of enlarged and lobed nuclei in arbusculated cells (Balestrini *et al*., 1992; Lingua *et al*.,
273 2001). Since nuclear enlargement may result from either chromatin decondensation (resulting in
274 increased transcriptional activity not affecting DNA content) or endoreduplication, we decided to
275 investigate ploidy levels in mycorrhizal and uninoculated root samples of *M. truncatula* by flow
276 cytometry. Unfortunately, analyses provided consistent results for uninoculated roots, but those
277 from mycorrhizal roots were not reliable due to nuclear aggregations and debris. Indeed,
278 microscopic observation of nuclei extracted from 35 days old mycorrhizal root segments revealed
279 the presence of abundant debris, likely derived from hyphal fragmentation and causing the flow
280 cytometer detector to malfunction.
281 Consequently, hypothesizing that nuclear changes were likely associated with pre-penetration
282 responses, we decided to focus our investigations on an earlier stage of AM colonization, when
283 intraradical fungal structures are restricted to fewer cells. To achieve this aim, we established in

vitro mycorrhizal root organ cultures (ROCs) of *M. truncatula* and *G. margarita*, where root colonization could be monitored (Chabaud *et al*., 2002) and short sub-hyphopodial segments with developing colonization units - including a few arbuscules - could be collected 3 days after hyphopodium formation.

Preliminary confocal imaging performed on 100µm-thick sections (Fig. 2a-d) confirmed nuclear enlargement in arbusculated cells, as previously observed in pot-grown *M. truncatula* (Fig. 1). Quantitative analysis confirmed that average areas and volumes were both significantly smaller (independent sample's median test, $P < 0.01$) in uninoculated compared to mycorrhizal ROCs (Fig. 2e,f). Average nuclear area changed from 36.4 ± 1.7 μm^2 in uninoculated to 49 ± 1.9 μm^2 in mycorrhizal samples, with corresponding changes in average nuclear volume (from 41.8 ± 3.2 μm^3 to 54 ± 3.1 μm^3). In agreement with our observations on whole plants, the frequency distribution of nuclear volumes for ROC samples (Supplemental Figure 2a) showed a significantly (Kruskal-Wallis test at $P < 0.01$) wider range in mycorrhizal (20 - 220 μm^3) than in uninoculated segments (20 - 145 μm^3).

Together, our analyses clearly showed that nuclear enlargement occurred during early stages of the interaction and was not limited to arbusculated cells, but extended to a few adjacent cells (Fig. 2 b,d), prompting us to further investigate this pattern.

G. margarita colonization causes local ploidy increase

We firstly applied flow cytometry to compare ploidy levels in PI-stained nuclei extracted from uninoculated and 3-day-old sub-hyphopodial segments (Fig. 3 a-b). Ploidy in uninoculated segments ranged from 2C to 32C (Fig. 3a), with 98.94% of 2C-4C nuclei and 1.06% of endoreduplicated nuclei, corresponding to 8C or higher ploidy. Importantly, only 8C and higher ploidy levels are reliable indicators of endoreduplication events, since the 4C class may include diploid cells caught in the G2 phase of mitosis at the moment of sampling (Vinardell *et al*., 2003).

By contrast, the range of ploidy in sub-hyphopodial segments reached as high as 256C (Fig. 3b) and a nearly three-fold increase (from 1.06% to 3.13%) was recorded in the percentage of endoreduplicated nuclei (above 8C). Increases were particularly conspicuous in 8C (two-fold), 16C (eleven-fold) and 32C (seven-fold) classes, deriving from two, three and four endoreduplication cycles, respectively. The occurrence of 64C, 128C and 256C nuclei was solely observed in sub-hyphopodial segments. Furthermore, the increase in endoreduplicated nuclei in mycorrhizal

315 samples corresponded to a decrease in the 4C class (from about 41% to 36%), suggesting that 4C
316 cells had undergone endoreduplication.
317 Following prior observations that nuclear enlargement was limited to arbusculated and adjacent
318 cortical cells, we imaged entire 1cm-long sub-hyphopodial root segments to better investigate this
319 pattern and determine how far this response extended along the root axis, in areas that were just
320 beyond the span of intraradical hyphae (Fig.4 a,b). This confirmed that the nuclear size increase was
321 focused on cortical cells in the colonized area and a majority of small nuclei was present in the
322 uncolonized ends of each root segment. We then used flow cytometry to analyze ploidy in the
323 central region of sub-hyphopodial segments (where most of the colonization had developed) and
324 compared it with the root segment ends, where no or very few intraradical hyphae were present
325 (Fig. 4 a,b).
326 This analysis (Figure 4 c,d) showed that 2.02% endoreduplicated nuclei (8C or higher ploidy) were
327 extracted from uncolonized ends (Fig. 4c), while this percentage raised to 3.43% in the central region
328 (Fig. 4d), with an almost two-fold increase in 8C, 16C, 32C, 64C and 128C classes.
329 Taken together, these results strongly suggest that the observed nuclear enlargement associated
330 with AM colonization is related to ploidy increases. Furthermore, such increases are strongly
331 focused on the colonized area. Lastly, the strict localization of ploidy changes in the vicinity of young
332 and expanding colonization units points to the activation of repeated endoreduplication cycles
333 alongside fungal propagation, and a consequent possible role for endoreduplication in the
334 accommodation response.
335
336 **Nuclear size and ploidy levels are unchanged in AM inoculated CSSP mutants**
337 To further test this hypothesis, we extended our analyses to uninoculated and inoculated ROCs from
338 *dmi2-2* and *dmi3-1 M. truncatula* mutants (Catoira *et al*., 2000; Morandi *et al*., 2005). In these
339 mutants, AM colonization is arrested at hyphopodium formation and no intraradical hyphae or
340 arbuscules develop under *in vitro* conditions (Genre *et al*., 2005). Image analysis of nuclear areas
341 and volumes in 3-day-old sub-hyphopodial segments showed no statistically significant change in
342 the nuclear populations from uninoculated and inoculated ROCs (Figure 5a-d). Similarly, no
343 difference (Kruskal-Wallis test, $P > 0.05$) was found between frequency distributions of nuclear
344 volumes (Supplemental Figure S2 b,c).
345 Flow cytometry-based ploidy analysis confirmed the absence of any significant increase in ploidy
346 levels between sub-hyphopodial and uninoculated root segments for any of the mutants (Fig. 6a-d).

The limited presence of higher ploidy levels in all mutant ROCs may be related to nuclei from the central cylinder, which appear larger in both mutant backgrounds compared to the wild-type. This aspect is further discussed in the next sections.

In conclusion, the lack of changes in nuclear size and ploidy in both CSSP mutants - where fungal penetration is arrested at the epidermal level - confirmed the association of nuclear enlargement and endoreduplication onset with fungal colonization of the root cortex.

Endocycle and S-phase markers are upregulated in wild-type inoculated roots

We then investigated the expression of endocycle markers and S phase-expressed genes in 3-day-old sub-hyphopodial root segments and corresponding uninoculated segments from wild-type, *dmi2-2* and *dmi3-1 M. truncatula* ROCs.

Firstly, we confirmed the occurrence (in wild-type) or lack of AM colonization (in both mutants) by analyzing the expression of two acknowledged plant symbiotic markers (Supplemental Figure 3a,b): the *Blue Copper-binding Protein MtBCBP* (Parádi *et al*., 2010), an early marker of cortex colonization and arbuscule development, and the *E3 ubiquitin ligase MtPUB1* (Vernié *et al*., 2016), an interactor of DMI2.

We then chose five acknowledged endocycle markers based on data in the literature. Two of them are negative regulators of G2-M-specific cyclins (Fig. 7a): *MtAPC/C subunit 2* (Tarayre *et al*., 2004), a member of the catalytic core in the plant Anaphase-Promoting Complex/Cyclosome (APC/C); and *MtCCS52A* (*Cell Cycle Switch Protein 52A*; Cebolla *et al*. 1999), a regulator of APC/C. The remaining three act during DNA replication in the S phase: *MtTOPO-VI A* (*MtVAG1)* and *MtTOPO-VI B* (Bergerat *et al*., 1994, 1997; Cortes & Pastor, 2003; Kondorosi & Kondorosi 2004), respectively the A and B subunits of DNA Topoisomerase VI; and *MtHist-H4* (Lepetit *et al*., 1992; Mariconti *et al*., 2002), a histone component of nucleosomes, required during DNA replication.

All five marker genes significantly increased their expression levels in mycorrhizal compared to uncolonized wild-type roots (Fig. 7b). By contrast, their transcript levels remained unchanged in the absence or presence of *G. margarita* hyphopodia, in both *dmi2-2* and *dmi3-1* mutants (Fig. 7b), with the exception of *MtTOPO-VI A*, which showed a decrease in *dmi2-2* and a small increase in *dmi3-1* inoculated roots.

In addition, the expression of the endocycle regulator *MtE2Fe/DEL1*, a DP/E2F-like transcription factor repressing CCS52A (Lammens *et al*., 2008), did not change upon AM inoculation of wild-type or *dmi2-2* and *dmi3-1* lines (Fig. 7b).

Furthermore, to check if an additional regulatory pathway repressing A2-type cyclins - and thus triggering endocycle - was activated in response to AM colonization, we analyzed the expression of *MtILP1* (De Veylder *et al*., 2011), a homolog protein to the C-terminal region of the mammalian GC-binding factor (Supplemental Figure 3c). *MtILP1* transcript level did not change significantly in control and mycorrhizal wild-type samples. However, its expression was upregulated in inoculated root segments of *dmi2-2* and *dmi3-1* mutants compared to their respective controls. This intriguing result suggests that this alternative endocycle pathway (Yoshizumi *et al*., 2006) - normally not triggered by AM in the wild-type - is activated in CSSP mutant background probably in response to *G. margarita* contact, downstream of CSSP-independent perception of AM fungal signals (Bonfante & Requena, 2011).

Overall, our gene expression results converge in supporting the occurrence of endoreduplication in root areas directly involved in AM fungal accommodation. In particular, the upregulation of key endocycle markers provides convincing molecular background to our observation of repeated rounds of endoreduplication in the vicinity of intraradical fungal structures.

A map of putative ploidy in *M. truncatula* roots

A reliable estimation of ploidy based on nuclear size is constrained by the fact that nuclear expansion may result from a combination of increases in DNA, protein or RNA content in the nucleoplasm. Nevertheless, a positive correlation between ploidy and nuclear size has been demonstrated in several plant tissues (Barrow, 2006; Bourdon *et al*., 2010; Robinson *et al*., 2018), especially in the case of repeated endoreduplication cycles (D'Amato, 1984; Joubés *et al*., 1999; Grandjean *et al*., 2004). We therefore decided to map out an atlas of nuclear size as a bona fide reporter of nuclear ploidy in longitudinal sections of uninoculated and inoculated *M. truncatula* roots, in an attempt to broaden our view of the correlation between fungal position and endoreduplication.

Firstly, we applied Sturges' rule (Sturges, 1926) to our data set of nuclear sizes in wild-type uninoculated and mycorrhizal ROC segments. This statistical analysis (see Materials and methods) identified five distinct classes in the population of nuclear areas from uninoculated samples (Fig. 8a), with average areas of 21.3 μm^2 (class I), 36.0 μm^2 (Class II), 52.4 μm^2 (Class III), 65.3 μm^2 (Class IV), 76.5 μm^2 (Class V), respectively. However, the Sturges analysis of mycorrhizal samples identified eight such classes (Fig. 8a) with respective sizes of 22.2 μm^2 (Class I), 39.6 μm^2 (Class II), 51.89 μm^2 (Class III), 66.7 μm^2 (Class IV), 82.17 μm^2 (Class V), 95.53 μm^2 (Class VI), 114.93 μm^2 (Class VII) and 127 μm^2 (Class VIII).

Notably, the five and eight nuclear classes - identified by applying descriptive statistics (Sturges, 1926) to our population of measurements - matched with the corresponding five and eight ploidy levels detected by flow cytometry. Moreover, the average nuclear area between classes showed a significant logarithmic positive correlation with the increase of the ploidy levels in both control ($r = 0.90$; $P < 0.05$) and mycorrhizal ($r = 0.85$; $P < 0.01$) sections (Fig. S4 a,b).

On this basis, we used this clustering to tag nuclei in our original images (Supplementary Figure S5) with different colors based on their size, obtaining maps of putative ploidy such as those shown in Figure 8 b,c. A detailed analysis of such maps from uninoculated roots (Fig. 8d) revealed that all epidermal nuclei belonged to classes I (29.1%) and II (0.3%) (Fig. 8b, red), while classes III, IV and V (Fig. 8b, orange) only appeared in cortical cells with percentages of 12.3%, 1.0% and 0.1%, respectively. This is in agreement with the expected polysomatic nature of *M. truncatula* roots (Kondorosi *et al*., 2000; Barrow & Meister, 2003).

The relative abundance of small nuclei (class I and II) in epidermal cells (24.3 % and 0.6%, respectively) was conserved in mycorrhizal root sections (Fig. 8d, Supplementary Figure S6 a). However, a larger population (19.3%) of class III, IV, V, VI, VII and VIII (13.0%, 4.0%, 1.5%, 0.6%, 0.1% and 0.1%, respectively) appeared in the cortex. Such large nuclei marked strictly the course of *G. margarita* hyphae (Fig. 8c, orange and yellow). In particular, enlarged nuclei concentrated in colonized cells (Fig. 8c; Supplementary Figure S6) and in the vicinity of intercellular hyphae (Supplementary Figure S6 b-e), with the largest classes (VI, VII and VIII) corresponding to arbusculated and neighboring cells (Fig 8c, Supplementary Figure S6 d-f).

In conclusion, even in the absence of direct evidence linking nuclear size and ploidy, our results provide indications that the ploidy increases described by flow cytometry correspond to the nuclear size increases observed by microscopy. Consequently, AM-related endoreduplication events appear to be restricted to the root cortex.

In contrast to the wild-type, the range of nuclear areas was unchanged in uninoculated and sub-hyphopodial segments from both *dmi2-2* and *dmi3-1* mutant lines (Fig. S5 c-f). In fact, Sturges' rule identified seven overlapping classes of nuclear areas in all four measurements of populations (Supplementary Figure S7 a). Similarly to the wild-type, we noted a full agreement between the number of nuclear classes and the number of ploidy levels detected by flow cytometry in both mutants (Fig. 6), where nuclear size increases also correlated ($r = 0.90$; $P < 0.01$) with the ploidy levels (Supplementary Figure S4 c-f). This scenario is represented in the maps presented in

Supplementary Figure S7 (b-e), where a comparable pattern of nuclear classes can be observed in both uninoculated and sub-hyphopodial segments of the two mutant lines.

Furthermore, we took advantage of the maps to analyze nuclear size in different cell types. As shown in Figure 9, average nuclear areas in epidermal cells were identical among control and inoculated roots of wild-type, *dmi2-2* and *dmi3-1* ROC lines (approximately 20 μm^2). The average nuclear areas of uncolonized cortical cells were also very similar between control and inoculated roots of the three ROC lines (approximately 40 μm^2). By contrast, the cortex of mycorrhizal wild-type roots displayed a pronounced increase in nuclear size for arbusculated cells (71.3 ± 10.3 μm^2) and a more moderate, but also statistically significant, increase in their neighboring uncolonized cortical cells (48.6 ± 4.3 μm^2).

In conclusion, detailed image analysis extended our understanding of nuclear responses to AM colonization of the root epidermal and cortical tissues, providing convincing evidence that size increases associated with fungal accommodation are limited to cortical cells that host fungal structures and those in their close vicinity, hinting at the activation of recursive endoreduplication events limited to the area of the root cortex where the fungus is accommodated.

DISCUSSION

Several microorganisms are known to manipulate the plant cell cycle machinery (Chandran & Wildermuth, 2016; Wildermuth *et al*., 2017), and growing evidence is in favor of a convergent evolution in both pathogenic and symbiotic plant interactions toward the promotion of host cell divisions and/or endoreduplication associated to microbe colonization (Wildermuth *et al*., 2010; Le Fevre *et al*., 2015; Chandran & Wildermuth, 2016).

Biotroph-induced tumors formed by mitotic proliferation are hallmarks of *Agrobacterium tumefaciens* (Gohlke & Deeken, 2014), *Ustilago maydis* (Brefort *et al*., 2009), and *Rice black-streak dwarf virus* (Shen *et al*., 2016). The powdery mildew *Golovinomyces orontii* induces host cell endoreduplication in *Arabisopsis thaliana* mesophyll cells hosting its feeding structures (Chandran *et al*., 2010; 2013). Plant parasitic root-knot nematodes form galls harboring polyploid multinucleated giant feeding cells associated with mitosis and endoreduplication reactivation (de Almeyda Engler & Gheysen, 2013; Kyndt *et al*., 2013; Siddique *et al*., 2015).

Mitosis and endocycle activation are also a feature of mutualistic interactions. Root nodule development in SNF requires the de novo formation of a meristem from dividing cortical cells (Xiao *et al*., 2014), and nodule cells that host N-fixing bacteroids go through several rounds of endoreduplication (Cebolla *et al*., 1999; Foucher & Kondorosi, 2000; Jones *et al*., 2007). Cell division and hypertrophy have also been reported in cortical and pericycle cells of *Casuarina glauca* (Laplaze *et al*., 2000) and *Ceanothus* (Berry & Sunnel, 1990) during intracellular and intercellular infection respectively, induced by *Frankia* hyphae (Tromas *et al*., 2013). Recently, ectopic cell divisions were detected in the cortex of AM colonized roots (Russo *et al*., 2019), while the occurrence of endoreduplication has so far been more difficult to assess, likely due to the transitory nature of fungal colonization and its asynchronous development.

AM colonization and local increases in ploidy

A hallmark of AM fungal accommodation is the profound reorganization of the host cell, starting from PPA assembly (Blancaflor *et al*., 2001; Genre *et al* 2008). Among these changes, cortical nuclei are reported to move to the cell center, and their associated size increase has previously been explained with possible endocycle activation (Berta *et al*., 2000; Fusconi *et al*., 2005; Bainard *et al*., 2011; Ivanof & Harrison 2014) and/or chromatin decondensation (Balestrini *et al*., 1992), linked to increased transcriptional activity (Genre *et al*., 2008; Gaude *et al*., 2012). Moreover, global increases in root ploidy upon AM colonization have been described in *Solanum lycopersicum* (Berta *et al*., 2000), *Pisium sativum L.* (Repetto *et al*., 2007), *Allium porrum* (Fusconi *et al*., 2005), and more recently in a number of angiosperm species (Bainard *et al*. 2011). Nevertheless, limited evidence is available of a correlation in time and space between nuclear changes and early stages of fungal accommodation.

In this scenario, our convergent results from flow cytometry, microscopy and gene expression analysis reveal that repeated rounds of endoreduplication are induced in *M. truncatula* roots as early as 48-60 hours after the formation of a *G. margarita* hyphopodium. Our novel and convincing evidence shows that this increase in ploidy levels is restricted to the root cortex, mainly to arbusculated and neighboring cells, anticipating fungal spread along the root axis.

While previous studies have been mostly focused on the analysis of relative changes in specific ploidy classes (e.g. 2C and 8C in Berta *et al*., 2000; 2C and 4C in Lingua *et al*., 2005), our analyses detected up to eight distinct classes, ranging between 2C and 256C. In agreement with Berta *et al*. (2000), we observed a slight decrease in 4C nuclei in colonized roots, which might correspond to

cortical cells that entered endoreduplication. In addition, we observed a strong increase in 8C, 16C and 32C classes for AM samples, and most notably the appearance of 64C, 128C and 256 C nuclei. This ability to resolve higher ploidy classes compared to previous research may be a consequence of our targeted sampling: selecting sub-hyphopodial segments may in fact have reduced the dilution of fewer populated high ploidy classes and possibly also improved the overall quality of nuclear extracts (de Almeida-Engler *et al*., 2016).

Furthermore, our detailed analysis of nuclear size distribution in longitudinal root sections and its correlation with ploidy revealed additional details. Firstly, epidermal cells do not appear to undergo endoreduplication, either prior to or following fungal penetration. This is in agreement with the conserved diploid status of root epidermal cells in most plants (Barrow, 2006) and the live observation of prepenetration responses to AM fungi, where nuclear enlargement has never been reported in the epidermis (Genre *et al*., 2008). Similarly, during rhizobial infection of legume roots, nuclear enlargement (and occasionally cell division) has been described in association with pre-infection threads in the root cortex (Van Brussel *et al*., 1992; Sieberer *et al*., 2012; Lace & Ott, 2018), but not in epidermal cells.

Consistent with cytometric and microscopic observations, our gene expression analyses revealed the upregulation of several key endocycle and S-phase markers during early AM colonization. The involvement of *CCS52* in AM, reported here, indicates the activation of the APC/C complex triggering the endocycle machinery during AM accommodation. Our data fit with previous reports of the involvement of CULLIN-4 during endocycle progression (Tahiri-Alaoui *et al*., 2002; Roodbarkelari *et al*., 2010). Based on the expression of *CCS52A* and *APC/C subunit 2*, we assume that the APC/C pathway controls endoreduplication in AM colonized roots 48 to 60 h after hyphopodium formation. Activation of *CCS52* genes has also been reported in plant hosts during rhizobium- (Cebolla *et al*., 1999; Vinardell *et al*., 2003; Roux *et al*., 2014; Suzaki *et al*., 2014; Yoon *et al*., 2014) and nematode- (Favery *et al*., 2002; de Almeida-Engler *et al*., 2012) interactions.

By contrast, the CCS52 repressor *MtE2F2-DEL1* was not upregulated in colonized roots, in agreement with previous studies (de Almeida-Engler *et al*., 2012), indicating a role for this gene in mitotically active (Lammens *et al*., 2008), but not endoreduplicating, cells (Vlieghe *et al*., 2005).

Signaling and ploidy increase

Interestingly, the extension of nuclear size increase to uncolonized cortical cells located in the vicinity of arbuscules and ahead of intraradical hyphal tips, suggests the presence of a yet

unidentified cell-to-cell signaling anticipating fungal arrival. These observations are in line with previous descriptions of cellular reorganization in the vicinity of colonized cortical cells (Blancaflor *et al*., 2001; Genre *et al*., 2008; Harrison, 2005). In this frame, CSSP-dependent activation of DELLA proteins was shown to induce the expression of genes involved in arbuscule development, such as *RAM1* and *RAD1* (Floss *et al*., 2013; Park *et al*., 2015; Takeda *et al*., 2015). Furthermore, Claeys *et al*. (2012) showed that DELLA proteins induce mitotic exit by modulating APC/C complex through down-regulation of *E2F-DEL1* (Pettkó-Szandtner *et al.,* 2006; De Veylder *et al*., 2007). In this scenario our observation of unchanged E2F-DEL1 expression in inoculated and uninoculated samples seem to exclude the involvement of this gene in AM-associated endocycle activation.

Nevertheless, our analyses of *dmi2-2* and *dmi3-1* mutants, indicating no change in nuclear size, ploidy or endocycle-related gene expression upon AM inoculation, provide indirect support for the involvement of signaling mechanisms. In fact, since CSSP-mediated signaling, PPA formation and fungal penetration are all absent in roots of both mutants, nuclear ploidy increase may be either directly induced by CSSP activation, or by the CSSP-dependent presence of fungal structures in the inner root tissues.

Along the same line, the expression of APC/C pathway-related genes confirms that endoreduplication is not induced by the AM fungus in either mutant. Only the *DNA topoisomerase VI subunit A* is differentially regulated in both inoculated mutants, with a decrease in transcript abundance for *dmi2-2* and an increase for *dmi3-1*. At present, this differential expression might be related to its function in another unidentified protein complex.

So far, our results in wild-type and mutant *M. truncatula* indicate endoreduplication as a key element of fungal accommodation-related processes in AM. This complements previous studies on the activation of cell division in the inner cortex of inoculated roots (Russo *et al*., 2019), overall supporting the hypothesis that cell cycle reactivation is required for symbiotic interface biogenesis through the redirection of the cell plate machinery. Although unpredicted, this process mirrors analogous mechanisms observed in several plant-microbe interactions and suggests that we are dealing with a conserved plant response to diverse biotrophic partners (Chandran & Wildermuth, 2016; Wildermuth et al., 2017; Lace & Ott, 2018).

ACKNOWLEDGEMENTS

We are grateful to Luisa Lanfranco, Valentina Fiorilli, Alessandra Salvioli and Paola Bonfante for fruitful discussion; to Danila Cabral do Nascimento for sharing ideas and suggestions and for her

help in the laboratory; to Julie Cazareth for her assistance with flow cytometry analyses; to Gilbert Engler and Olivier Pierre for their support and criticisms to confocal microscopy; and to Dan Chamberlain for revising the English language. We also thank Mara Novero and Antonella Faccio for their friendly support and technical assistance during sample preparation. Lastly, we are grateful to the anonymous reviewers for their constructive contribution to improve the quality of our manuscript. GC was supported by a PhD fellowship from the Italian Ministry of University and Research. Financial support for this research was granted by Compagnia di Sanpaolo (project REPROGRAM – Progetti di Ateneo 2012, Call 01; University of Turin (Ricerca locale 2015-2017); COST Action FA1206, Short Term Scientific Missions.

AUTHOR CONTRIBUTIONS

GC designed the experiments, performed microscopy, image analysis, flow cytometry and gene expression analyses, and wrote the text. VV performed gene expression analyses and contributed to the experimental set-up and text writing. GR carried out preliminary gene expression analyses and contributed to designing the research and writing the text. MP prepared pot cultures and samples for molecular analyses. IS performed statistical and image analyses. JdAE contributed to experimental design and text writing. AG designed the research and experiments and wrote the text.

REFERENCES

Bainard LD, Bainard JD, Newmaster SG, Klironomos JN. 2011. Mycorrhizal symbiosis stimulates endoreduplication in angiosperms. *Plant Cell Environ*. 34: 1577–1585.

Balestrini R, Berta G, Bonfante P. 1992. The plant nucleus in mycorrhizal roots: positional and structural modifications. *Biol. Cell* 75: 235–243.

Barow M. 2006. Endopolyploidy in seed plants. *BioEssays*. 28:271-281.

Barow M, Meister A. 2003. Endopolyploidy in seed plants is differently correlated to systematics, organ, life strategy and genome size. *Plant Cell Environ*. 26:571-584.

Bécard G, Fortin JA. 1988. Early events of vesicular–arbuscular mycorrhiza formation on Ri T-DNA transformed roots. *New Phytol*. 108:211–218.

Bergerat A, de Massy B, Gadelle D, Varoutas PC, Nicolas A, and Forterre P. 1997. An atypical topoisomerase II from Archaea with implications for meiotic recombination. *Nature* 386: 414–417.

Bergerat A, Gadelle D, Forterre P. 1994. Purification of a DNA topoisomerase II from the hyperthermophilic archaeon *Sulfolobus shibatae*. A thermostable enzyme with both bacterial and eucaryal features. *J. Biol. Chem*. 269: 27663–27669.

Berry AL, Sunnel LA. 1990. The infection process and nodule development. In *The biology of Frankia and actinorhizal plants*. Schwintzer CR, Tjepkema JD (eds). Academic, New York, NY, pp 61–81.

Berta G, Fusconi A, Sampò S, Lingua G, Perticone S, Repetto O. 2000. Polyploidy in tomato roots as affected by arbuscular mycorrhizal colonization. *Plant and Soil* 226: 37–44.

Blancaflor E, Zhao L, Harrison M. 2001. Microtubule organization in root cells of *Medicago truncatula* during development of an arbuscular mycorrhizal symbiosis with *Glomus versiforme*. *Protoplasma* 217: 154–165.

Bolte S, Cordelieres FP. 2006. A guided tour into subcellular colocalization analysis in light microscopy. *J. Microsc*. 224:213–232.

Bonfante P, Requena N. 2011. Dating in the dark: How roots respond to fungal signals to establish arbuscular mycorrhizal symbiosis. *Curr. Opin. Plant Biol*. doi: 10.1016/j.pbi.2011.03.014.

Bourdon M, Frangne N, Mathieu-Rivet E, Nafati M, Cheniclet C, Renaudin J-P, Chevalier C. 2010. Endoreduplication and growth of fleshy fruits. *Prog. Bot*. 71:101–132.

Brefort T, Doehlemann G, Mendoza-Mendoza A, Reissmann S, Djamei A, Kahmann R. 2009. *Ustilago maydis* as a pathogen. *Annu. Rev. Phytopathol*. 47:423–45.

Buschhorn BA, Peters JM. 2006. How APC/C orders destruction. *Nat Cell Biol.* 8: 209–211.

Catoira R, Galera C, de Billy F, Penmetsa RV, Journet EP, Maillet F, Rosenberg C, Cook D, Gough C, Dénarié J. 2000. Four genes of *Medicago truncatula* controlling components of a Nod factor transduction pathway. *Plant Cell* 12:1647–1665.

Cavallini A, Baroncelli S, Lercari B, Cionini G, Rocca M, D'Amato F. 1995. Effect of light and gibberellic acid on chromosome endoreduplication in leaf epidermis of *Triticum durum* Desf. *Protoplasma*. 186:57-62.

Cebolla A, Vinardell JM, Kiss E, Oláh B, Roudier F, Kondorosi A, Kondorosi E. 1999. The mitotic inhibitor ccs52 is required for endoreduplication and ploidy-dependent cell enlargement in plants. *EMBO J*. 18:4476–84

Chabaud M, Genre A, Sieberer BJ, Faccio A, Fournier J, Novero M, Barker DG, Bonfante P. 2011. Arbuscular mycorrhizal hyphopodia and germinated spore exudates trigger Ca^{2+} spiking in the legume and nonlegume root epidermis. *New Phytol*. 189:347–355.

Chabaud M, Venard C, Defaux-Petras A, B ecard G, Barker DG. 2002. Targeted inoculation of *Medicago truncatula* in vitro root cultures reveals *MtENOD11* expression during early stages of infection by arbuscular mycorrhizal fungi. *New Phytol*. 156:265–273.

Chandran DC, Wildermuth M. 2016. Modulation of host endocycle during plant biotroph interactions. In The Enzymes, ed. C Lin, S Luan, Vol. 40, pp. 65–103, Burlington, MA: Academic.

Chandran D, Rickert J, Cherk C, Dotson BR, Wildermuth MC. 2013. Host cell ploidy underlying the fungal feeding site is a determinant of powdery mildew growth and reproduction. *Mol. Plant-Microbe Interact*. 26:537–45.

Chandran D, Inada N, Hather G, Kleindt CK, Wildermuth MC. 2010. Laser microdissection of *Arabidopsis* cells at the powdery mildew infection site reveals site-specific processes and regulators. *PNAS* 107:460–65.

Claeys H, Skirycz A, Maleux K, Inzé D. 2012. DELLA signaling mediates stress-induced cell differentiation in *Arabidopsis* leaves through modulation of anaphase-promoting complex/cyclosome activity. *Plant Physiol*. 159:739-747.

Cortes F, Pastor N. 2003. Induction of endoreduplication by topoisomerase II catalytic inhibitors. *Mutagenesis* 18(2):105-112.

D'Amato F. 1984. Role of polyploidy in reproductive organs and tissues. *In Embryology of Angiosperms (BM, J., ed.)*. New York: Springer, pp. 519– 566.

de Almeida-Engler J, de Siqueira KMS, do Nascimento DC, da Costa TG, Engler G. 2016. A cellular outlook of galls induced by root-knot nematodes in the model host *Arabidopsis thaliana*. *Nematoda* 6. ed. http://dx.doi.org/10.4322/nematoda.00616.

de Almeida Engler J, Gheysen G. 2013. Nematode-induced endoreduplication in plant host cells: Why and how? Mol. *Plant-Microbe Interact*. 26:7–24.

de Almeida-Engler J, Kyndt T, Vieira P, Van Cappelle E, Boudolf V, Sanchez V, Escobar C, De Veylder L, Engler G, Abad P *et al*. 2012. *CCS52* and *DEL1* genes are key components of the endocycle in nematode-induced feeding sites. *Plant J*. 72:185–98.

de Veylder L, Larkin JC, Schnittger A. 2011. Molecular control and function of endoreplication in development and physiology. *Trends Plant. Sci*. 16:624–34.

De Veylder L, Beeckman T, Inzé D. 2007. The ins and outs of the plant cell cycle. *Nat. Rev. Mol. Cell Biol*. 8:655–665.

Dörmann P, Kim H, Ott T, Schulze-Lefert P, Trujillo M, Wewer V, Huckelhoven R. 2014. Cell-autonomous defense, re-organization and trafficking of membranes in plant-microbe interactions. *New Phytol*. 204, 815–822.

Engelen-Eigles G, Jones RJ, Phillips RL. 2000. DNA endoreduplication in maize endosperm cells: the effect of exposure to short-term high temperature. *Plant Cell Environ*. 23:657 – 663.

Favery B, Complainville A, Vinardell JM, Lecomte P, Vaubert D, Mergaert P, Kondorosi A, Kondorosi E, Crespi M, Abad P. 2002. The endosymbiosisinduced genes *ENOD40* and *CCS52a* are involved in endoparasitic-nematode interactions in *Medicago truncatula*. *Mol. Plant Microbe Interact*. 15:1008–1013.

Floss DS, Levy JG, Le ́vesque-Tremblay V, Pumplin N, Harrison MJ. 2013. DELLA proteins regulate arbuscule formation in arbuscular mycorrhizal symbiosis. *Proc. Natl. Acad. Sci*. USA 110: E5025–E5034.

Foucher F, Kondorosi E. 2000. Cell cycle regulation in the course of nodule organogenesis in *Medicago*. *Plant Mol. Biol*. 43:773–786.

Fusconi A, Lingua G, Trotta A, Berta G. 2005. Effects of arbuscular mycorrhizal colonization and phosphorus application on nuclear ploidy in *Allium porrum* plants. *Mycorrhiza* 15: 313–321.

Gage DJ. 2004. Infection and invasion of roots by symbiotic, nitrogen fixing rhizobia during nodulation of temperate legumes. *Microbiol. Mol. Biol. Rev.* 68, 280–300.

Galli MG. 1988*.* The role of DNA synthesis during hypocotyl elongation in light and dark. *Annals of Botany.* 62:287-293*.*

Gaude N, Bortfeld S, Duensing N, Lohse M, Krajinski F. 2012. Arbuscule-containing and non-colonized cortical cells of mycorrhizal roots undergo extensive and specific reprogramming during arbuscular mycorrhizal development. *Plant Journal* 69: 510–528.

Genre A, Chabaud M, Balzergue C, Puech-Page`s V, Novero M, Rey T, Fournier J, Rochange S, Bécard G, Bonfante P *et al*. 2013. Short-chain chitin oligomers from arbuscular mycorrhizal fungi trigger nuclear Ca^{2+} spiking in *Medicago truncatula* roots and their production is enhanced by strigolactone. *New Phytol*. 198:190–202.

Genre A, Chabaud M, Faccio A, Barker DG, Bonfante P. 2008. Prepenetration apparatus assembly precedes and predicts the colonization patterns of arbuscular mycorrhizal fungi within the root cortex of both *Medicago truncatula* and *Daucus carota*. *Plant Cell* 20: 1407–1420.

693 **Genre A, Chabaud M, Timmers T, Bonfante P, Barker DG. 2005.** Arbuscular mycorrhizal fungi elicit
694 a novel intracellular apparatus in *Medicago truncatula* root epidermal cells before infection. *Plant*
695 *Cell* 17: 3489–3499.
696 **Giovannetti M, Sbrana C, Avio L, Citernesi AS, Logi C. 1993.** Differential hyphal morphogenesis in
697 arbuscular mycorrhizal fungi during preinfection stages. *New Phytol*. 125:587-593.
698 **Gohlke J, Deeken R. 2014**. Plant responses to *Agrobacterium tumefaciens* and crown gall
699 development. *Front. Plant Sci*. 5:155.
700 **Grandjean O, Vernoux T, Laufs P, Belcram K, Mizukami Y, Traas J. 2004.** In Vivo analysis of cell
701 division, cell growth, and differentiation at the shoot apical meristem in *Arabidopsis*. *Plant Cell*,
702 16:74–87.
703 **Gutjahr C, Parniske M. 2013.** Cell and developmental biology of the arbuscular mycorrhiza
704 symbiosis. *Annu. Rev. Cell Dev. Biol*. 29: 593–617.
705 **Hammer Ø, Harper DAT, Ryan PD. 2004**. Past: paleontological statistics software package for
706 education and data analysis. *Palaeontologia Electronica* 4, art. 4
707 **Harper JW, Burton JL, Solomon MJ. 2002.** The anaphase-promoting complex: it's not just for mitosis
708 any more. *Genes Dev*. 16:2179-2206.
709 **Harrison M. 2005.** Signaling in the mycorrhizal symbiosis. *Annu. Rev. Microbiol*. 59: 19–42.
710 **Hewitt EJ. 1966.** "Sand and water culture methods used in the study of plant nutrition," in Technical
711 Communication No. 22 (Kent: Commonwealth Agriculture Bureau), 431–432.
712 **Heyman J, de Veylder L. 2012**. The anaphase-promoting complex/cyclosome in control of plant
713 development. *Mol. Plant*. 5:1182–94.
714 **Hohnjec N, Vieweg MF, Pühler A, Becker A, Küster H. 2005**. Overlaps in the transcriptional profiles
715 of *Medicago truncatula* roots inoculated with two different *Glomus* fungi provide insights into the
716 genetic program activated during arbuscular mycorrhiza. *Plant Physiol*. 137, 1283–1301.
717 **Ivanov S, Harrison MJ. 2014**. A set of fluorescent protein-based markers expressed from
718 constitutive and arbuscular mycorrhiza-inducible promoters to label organelles, membranes and
719 cytoskeletal elements in *Medicago truncatula*. *Plant J*. 80: 1151–1163.
720 **Jones KM, Kobayashi H, Davies BW, Taga ME, Walker GC. 2007**. How rhizobial symbionts invade
721 plants: the *Sinorhizobium-Medicago* model. *Nat. Rev. Microbiol*. 5:619–33.
722 **Joubés J, Phan T-H, Just D, Rothan C, Bergounioux C, Raymond P, Chevalier C. 1999.** Molecular and
723 biochemical characterization of the involvement of cyclin-dependent kinase CDKA during the early
724 development of tomato fruit. *Plant Physiol*. 121:857–869.

Kalve S, De Vos D, Beemster GTS. 2014. Leaf development: a cellular perspective. *Front. Plant Sci., 5:362.*

Kondorosi E, Kondorosi A. 2004. Endoreduplication and activation of the anaphase-promoting complex during symbiotic cell development. *FEBS Lett*. 567:152–57.

Kondorosi E, Roudier F, Gendreau E. 2000. Plant cell-size control: growing by ploidy? *Curr. Opin. Plant Biol.* 3:488–492.

Kormanik PP, McGraw AC. 1982. Quantification of vesicular–arbuscular mycorrhizae in plant roots. In: Schenk NC, ed. Methods and principles of mycorrhizal research. St Paul, MN, USA: American Phytopathological Society, 37–45.

Kruskal WH, Wallis WA. 1952. Use of ranks in one-criterion variance analysis. *Journal of the American Statistical Association* 47: 583–621.

Kyndt T, Vieira P, Gheysen G, de Almeida-Engler J. 2013. Nematode feeding sites: unique organs in plant roots. *Planta* 238:807–18.

Lace B, Ott T. 2018. Commonalities and Differences in Controlling Multipartite Intracellular Infections of Legume Roots by Symbiotic Microbes. *Plant Cell Physiol.* 59: 666–677.

Lanfranco L, Novero M, Bonfante P. 2005. The mycorrhizal fungus *Gigaspora margarita* possesses a CuZn superoxide dismutase that is up-regulated during symbiosis with legume hosts. *Plant Physiol*. 137:1319–1330.

Lammens T, Boudolf V, Kheibarshekan L, Zalmas LP, Gaamouche T, Maes S, Vanstraelen M, Kondorosi E, La Thanghue NB, Govaerts W et al. 2008. Atypical E2F activity restrains APC/CCCS52A2 function obligatory for endocycle onset. *PNAS* 105:14721–26.

Laplaze L, Duhoux E, Franche C, Frutz T, Svistoonoff S, Bisseling T, Bogusz D, Pawlowski K. 2000. *Casuarina glauca* prenodule cells display the same differentiation as the corresponding nodule cells. *Mol Plant Microbe Interact* 13:107–112.

Lepetit M, Ehling M, Chaubet N, Gigot C. 1992. A plant histone gene promoter can direct both replication-dependent and -independent gene expression in transgenic plants. *Mol. Gen. Genet*. 231:276-285.

Le Fevre R, Evangelisti E, Rey T, Schornack S. 2015. Modulation of host cell biology by plant pathogenic microbes. *Annu. Rev. Cell Dev. Bio.* 31:201–29.

Lingua G, Trotta A, Prigione V, Ugoccioni R, Berta G. 2005. Nucleus size in the host cells of an Arbuscular Mycorrhizal system: a mathematical approach to estimate the role of ploidy and chromatin condensation. *Caryologia* 58:112–121.

Lingua G, Fusconi A, Berta G. 2001. The nucleus of differentiated root plant cells: modifications induced by arbuscular mycorrhizal fungi. *Eur J Histochem*. 45(1):9-20.

McLean AM, Bravo A, Harrison MJ. 2017. Plant Signaling and Metabolic Pathways Enabling Arbuscular Mycorrhizal Symbiosis. *Plant Cell* 29: 2319–2335. doi:10.1105/tpc.17.00555.

Mariconti L, Pellegrini B, Cantoni R, Stevens R, Bergounioux C, Cella R, Albani D. 2002. The E2F Family of Transcription Factors from *Arabidopsis thaliana*. *J. Biol. Chem*., 277, 9911–9919.

Morandi D, Prado E, Sagan M, Duc G. 2005. Characterisation of new symbiotic *Medicago truncatula* (Gaertn.) mutants, and phenotypic or genotypic complementary information on previously described mutants. *Mycorrhiza* 15:283–289.

Musialak T, Siane D, Liebig C, Bayer M. 2016. A Versatile Optical Clearing Protocol for Deep Tissue Imaging of Fluorescent Proteins in *Arabidopsis thaliana*. *PLoS ONE*, 11, e0161107.

Oldroyd GED. 2013. Speak, friend, and enter: signaling systems that promote beneficial symbiotic associations in plants. *Nature Reviews Microbiology* 11: 252–263.

Parádi I, van Tuinen D, Morandi D, Ochatt S, Robert F, Jacas L, Dumas-Gaudot E. 2010. Transcription of two blue copper-binding protein isogenes is highly correlated with arbuscular mycorrhizal development in *Medicago truncatula*. *Mol Plant Microbe Interact* 23:1175-1183.

Park HJ, Floss DS, Levesque-Tremblay V, Bravo A, Harrison MJ. 2015. Hyphal branching during arbuscule development requires Reduced Arbuscular Mycorrhiza1. *Plant Physiol*. 169:2774–2788.

Parniske M. 2008. Arbuscular mycorrhiza: the mother of plant root endosymbioses. *Nature Reviews Microbiology* 6: 763–775.

Pettkó-Szandtner A, Mészáros T, Horváth GV, Bakó L, Csordás-Tóth E, Blastyák A, Zhiponova M, Miskolczi P, Dudits D. 2006. Activation of an alfalfa cyclin-dependent kinase inhibitor by calmodulin-like domain protein kinase. *Plant J*. 46:111–123.

Pumplin N, Harrison MJ. 2009. Live-cell imaging reveals periarbuscular membrane domains and organelle location in *Medicago truncatula* roots during arbuscular mycorrhizal symbiosis. *Plant Physiology* 151: 809–819.

Rasmussen R. 2001. Quantification on the LightCycler instrument. In: Meuer S, Wittwer C, Nakagawara K, eds. Rapid cycle real-time PCR: methods and applications. Heidelberg, Germany: Springer-Verlag, 21–34.

Repetto O, Massa N, Gianinazzi-Pearson V, Dumas-Gaudot E, Berta G. 2007. Cadmium effects on populations of root nuclei in two pea genotypes inoculated or not with the arbuscular mycorrhizal fungus *Glomus mosseae*. *Mycorrhiza.* 17:111-120.

Robinson DO, Coate JE, Singh A, Hong L, Bush MS, Doyle JJ, Roeder AHK. 2018. Ploidy and size in the *Arabidopsis* sepal. *Plant Cell*, doi: 10.1105/tpc.18.00344.

Roodbarkelari F, Bramsiepe J, Weinl C, Marquardt S, Novak B, Jakobi MJ, Lechner E, Genschik P, Schnittger A. 2010. Cullin 4-ring finger-ligase plays a key role in the control of endoreplication cycles in *Arabidopsis* trichomes. *PNAS* 107:15275–80.

Roux B, Rodde N, Jardinaud MF, Timmers T, Sauviac L, Cottret L, Carrére S, Sallet E, Courcelle E, Moreau S *et al*. 2014. An integrated analysis of plant and bacterial gene expression in symbiotic root nodules using laser-capture microdissection coupled to RNA sequencing. *Plant J*. 77:817–37.

Russo G, Carotenuto G, Fiorilli V, Volpe V, Chiapello M, Van Damme D, Genre A. 2019. Ectopic activation of cortical cell division during the accommodation of arbuscular mycorrhizal fungi. *New Phytol*. doi: 10.1111/nph.15398.

Salvioli A, Bonfante P. 2013. Systems biology and "omics" tools: a cooperation for next-generation mycorrhizal studies. *Plant Sci* 203: 107–114.

Shapiro SS, Wilk MB. 1965. An analysis of variance test for normality (complete samples). *Biometrika* 52: 591–611.

Shen J, Chen X, Chen J, Sun L. 2016. A phloem-limited fijivirus induces the formation of neoplastic phloem tissues that house virus multiplication in the host plant. *Sci. Rep*. 6:29848.

Siddique S, Radakovic Z, de la Torre CM, Chronis D, Nová k O, Ramireddy E, Holbein J, Matera C, Hutten M, Gütbrod P *et al*. 2015. A parasitic nematode releases cytokinin that controls cell division and orchestrates feeding site formation in host plants. *PNAS* 112:12669–74.

Sieberer BJ, Chabaud M, Fournier J, Antonius CJ, Barker T, Barker DG. 2012. A switch in Ca^{2+} spiking signature is concomitant with endosymbiotic microbe entry into cortical root cells of *Medicago truncatula*. *Plant J.* 69:822-830.

Sieberer BJ, Chabaud M, Timmers AC, Monin A, Fournier J, Barker DG. 2009. A nuclear-targeted cameleon demonstrates intranuclear Ca^{2+}spiking in *Medicago truncatula* root hairs in response to rhizobial nodulation factors. *Plant Physiol*. 151:1197–1206.

Smith SE and Read DJ. 1997. Mycorrhizal Symbiosis. *Academic Press*, London, New York, 1-605.

Smulders MJM, Rus-Kortekaas W, Gilissen LJW. 1994. Development of polysomaty during differentiation in diploid and tetraploid tomato (*Lycopersicon esculentum*) plants. *Plant Science* 97:53–60.

Spatafora JW, Chang Y, Benny GL, Lazarus K, Smith ME, Berbee ML *et al*. 2016. A phylum-level phylogenetic classification of zygomycete fungi based on genome-scale data. *Mycologia* 108: 1028–1046.

Sturges HA. 1926. Choice of a Class Interval. Journal of the American Statistical Association, Vol. 21, No. 153, pp. 65-66.

Suzaki T, Ito M, Yoro E, Sato S, Hirakawa H, Takeda N, Kawaguchi M. 2014. Endoreduplication-mediated initiation of symbiotic organ development in *Lotus japonicus*. *Development* 141:2441–45.

Tahiri-Alaoui A, Lingua G, Avrova A, Sampò S, Fusconi A, Antoniw J, Berta G. 2002. A cullin gene is induced in tomato root forming arbuscular mycorrhizae. *Can. J. Bot*. 80:607–16.

Takeda N, Handa Y, Tsuzuki S, Kojima M, Sakakibara H, Kawaguchi M. 2015. Gibberellins interfere with symbiosis signaling and gene expression and alter colonization by arbuscular mycorrhizal fungi in *Lotus japonicus*. *Plant Physiol*. 167:545–557.

Tarayre S, Vinardell JM, Cebolla A, Kondorosi A, Kondorosi E. 2004. Two Classes of the Cdh1-Type Activators of the Anaphase-Promoting Complex in Plants: Novel Functional Domains and Distinct Regulation. *Plant Cell*. 16:422-434.

Tromas A, Diagne N, Diedhiou I, Prodjinoto H, Cissoko M, Crabos A, Diouf D, Sy MO, Champion A, Laplaze L. 2013. Establishment of Actinorhizal symbioses. In the *Symbiotic Endophytes*, R. Aroca (ed.), Soil Biology, Vol. 37, pp. 89-101, Berlin Heidelberg, Springer-Verlag.

Truchet, G. 1978. Sur l'état diploide des cellules du méristème des nodules radiculaires de Légumineuses. *Ann. Sci. Nat., Bot. Biol. Vég*. 19, 3–38.

Van Brussel AA, Bakhuizen R, van Spronsen PC, Spaink HP, Tak T, Lugtenberg BJ, Kijne JW. 1992. Induction of pre-infection thread structures in the leguminous host plant by mitogenic lipo-oligosaccharides of *Rhizobium*. *Science*. 2547:70–72.

Van Oostveldt P, van Parijs RB. 1975. Effect of light on nucleic-acid synthesis and polyploidy level in elongating epicotyl cells of *Pisum sativum*. *Planta* 124:287-295.

Vernie T, Camut S, Camps C, Rembliere C, de Carvalho-Niebel F, MbengueM, Timmers T, Gasciolli V, Thompson R, le Signor C et al. 2016. PUB1interacts with the receptor kinase DMI2 and negatively regulates rhizobial and arbuscular mycorrhizal symbioses through Its ubiquitination activity in *Medicago truncatula*. *Plant Physiology* 170:2312–2324.

Vieira P, Escudero C, Rodiuc N, Boruc J, Russinova E, Glab N, Mota M, De Veylder L, Abad P, Engler G *et al*. 2013. Ectopic expression of Kip-related proteins restrains root-knot nematode-feeding site expansion. *New Phytol*. 199:505–19.

Vieira P, Engler G, de Almeida Engler J. 2012. Whole-mount confocal imaging of nuclei in giant feeding-cells induced by root-knot nematodes in *Arabidopsis*. *New Phytol*. 195: 488–496.

Vinardell JM, Fedorova E, Cebolla A, Kevei Z, Horvath G, Kelemen Z, Tarayre S, Roudier F, Mergaert P, Kondorosi A *et al*. 2003. Endoreduplication mediated by the anaphase-promoting complex activator CCS52A is required for symbiotic cell differentiation in *Medicago truncatula* nodules. *Plant Cell.* 15:2093-105.

Vlieghe K, Boudolf V, Beemster GTS, Maes S, Magyar Z, Atanassova A, de Almeida-Engler J, De Groodt R, Inzé D, De Veylder L *et al*. 2005. The DP-E2F-like DEL1 gene controls the endocycle in *Arabidopsis thaliana*. *Curr. Biol*. 15:59–63.

Wildermuth MC, Steinwand MA, McRae AG, Jaenisch J, Chandran D. 2017. Adapted Biotroph Manipulation of Plant Cell Ploidy. *Annu. Rev. Phytopathol*. 55:537–564.

Wildermuth MC. 2010. Modulation of host nuclear ploidy: a common plant biotroph mechanism. *Curr. Opin. Plant Biol*. 13:449–58.

Xiao TT, Schilderink S, Moling S, Deinum EE, Kondorosi E, Franssen H, Kulikova O, Niebel A, Bisseling T. 2014. Fate map of *Medicago truncatula* root nodules. *Development* 141, 3517e3528.

Yoon HJ, Hossain MS, Held M, Hou H, Kehl M, Tromas A, Sato S, Tabata S, Andersen SU, Stougaard J *et al*. 2014. *Lotus japonicus* SUNERGOS1 encodes a predicted subunit A of a DNA topoisomerase VI that is required for nodule differentiation and accommodation of rhizobial infection. *Plant J*. 78:811–21.

Yoshizumi T, Tsumoto Y, Takiguchi T, Nagata N, Yamamoto YY, Kawashima M, Ichikawa T, Nakazawa M, Yamamoto N, Matsui M. 2006. INCREASED LEVEL OF POLYPLOIDY1, a Conserved Repressor of CYCLINA2 Transcription, Controls Endoreduplication in *Arabidopsis. Plant Cell.* 18:2452-2468.

Zhang C, Gong FC, Lambert GM, Galbraith DW. 2005. Cell type-specific characterization of nuclear DNA contents within complex tissues and organs. *Plant Methods* 1, 7.

877 **SUPPORTING INFORMATION**

878 **Method S1.** Nuclear staining for confocal imaging

879 **Method S2.** Image analysis of nuclear size

880 **Table S1.** List of primers used in this work.

881 **Figure S1.** Frequency distribution of nuclear areas and volumes in control and mycorrhizal roots of
882 *M. truncatula*.

883 **Figure S2**. Frequency distribution of nuclear volumes in uninoculated and inoculated ROCs of wild-
884 type, *dmi2-2* and *dmi3-1 M. truncatula*.

885 **Figure S3.** Gene expression analysis of mycorrhizal markers *MtBCBP* and *MtPUB1*, and the
886 alternative endocycle regulator *MtILP1* in ROC segments sampled 48-60 hours after hyphopodium
887 development.

888 **Figure S4.** Correlation between nuclear classes (y-axis) and ploidy levels (x-axis).

889 **Figure S5.** Maximum brightness projections of confocal z-stacks from DAPI-stained wild-type, *dmi2-*
890 *2* and *dmi3-1* ROC segments.

891 **Figure S6.** Increase in nuclear areas throughout root colonization.

892 **Figure S7.** Maps of putative ploidy in uninoculated and inoculated ROC segments from *dmi2-2* and
893 *dmi3-1* mutants.

894

895

896 **FIGURE LEGENDS**

897

898 **Fig. 1. Analysis of nuclear size in uninoculated and mycorrhizal roots of *M. truncatula*.**
899 Representative confocal images (z-stack projections) of longitudinal root sections from pot grown
900 *M. truncatula* stained with DAPI to visualize nuclear morphology (a,b) and acid fuchsin (c,d) to
901 highlight intraradical hyphae (hy) and arbuscules (ar). DAPI staining revealed an apparent increase
902 in nuclear size (b, white arrows) for all colonized cortical cells from mycorrhizal roots. After the
903 comparison with fuchsin-stained samples, intraradical fungal structures are easily recognizable in
904 DAPI images by their numerous small nuclei (asterisks) and a diffuse background fluorescence. Scale
905 bars = 50 μm.
906 Histograms in (e,f) report average nuclear areas (e) and volumes (f) as estimated through image
907 analysis of 2052 and 2222 DAPI-stained nuclei from 20 uninoculated and 20 mycorrhizal root
908 segments respectively. Colonization of cortical cells produced a significant increase in both nuclear

areas and volumes. Bars represent standard errors; asterisks indicate statistically significant differences based on independent sample median tests for data with non-normal distribution ($P < 0.01$). *G. m.* = *Gigaspora margarita*.

Fig. 2. Analysis of nuclear size in uninoculated and mycorrhizal *M. truncatula* ROCs. Representative images of longitudinal sections stained with DAPI (green, a, b) and SR2200 (gold, c, d) show nuclear and cell wall morphology in uninoculated (a, c) and mycorrhizal (b, d) segments of root organ cultures (ROCs). Large nuclei were found in arbusculated cells (white arrows) and some of the neighboring cortical cells (red arrows), compared to the smaller nuclei of distant cortical cells (white arrowheads), which were comparable in size to those observed in uninoculated roots (a, c). Small-sized fungal nuclei are evident in hyphae and arbuscules (asterisks). DAPI-SR2200 counter-staining (c, d) provided a clearer labeling of plant and fungal (ar) walls, confirming the increase in nuclear size (white arrows) of arbusculated versus uncolonized cortical cells (arrowheads). Scale bars = 50 μm.

Histograms in (e) report average areas of 3600 and 3850 DAPI-stained nuclei from 25 uninoculated and 25 mycorrhizal root segments respectively. Histograms in (f) represent average calculated volumes of 2000 and 2449 nuclei from the same respective samples. Both nuclear areas and volumes significantly increased in mycorrhizal compared to uninoculated ROCs. Bars represent standard errors; asterisks indicate statistically significant differences based on independent sample median tests ($P < 0.01$). *G. m*. = *Gigaspora margarita*.

Fig. 3. Analysis of ploidy by flow cytometry in uninoculated and mycorrhizal *M. truncatula* ROC segments. The majority of nuclei in uninoculated segments (a) consisted of 2C and 4C nuclei (98.94%), while endoreduplicated nuclei (8C, 16C and 32C) represented 1.06% of extracted nuclei. By contrast, a three-fold increase in the percentage of endoreduplicated nuclei (3.13%) and the appearance of higher ploidy classes (64C, 128C and 256C) was recorded in mycorrhizal (sub-hyphopodial) segments. Chi-Square analysis identified a significant difference between percentages of endoreduplicated nuclei (above 8C) in uninoculated and mycorrhizal root segments ($P < 0.01$). Histograms report average values from three independent experiments; error bars represent standard deviations. *G. m*. = *Gigaspora margarita*.

940 **Fig. 4. Analysis of ploidy in central versus terminal zones of sub-hyphopodial *M. truncatula* ROC**
941 **segments.** The scheme in (a) represents a typical infection unit in 48-60 h old sub-hyphopodial
942 segments of *M. truncatula*, with a patch of hyphae and arbuscules (ar) in the central zone, directly
943 underneath the hyphopodium (hp), and very few intraradical fungal structures in either terminal
944 end of the segment. Panels in (b) display corresponding confocal images from a DAPI-stained ROC
945 segment. Larger nuclei (arrows) were more abundant in the central zone than in terminal ends, and
946 characterized cells that were either colonized or adjacent to the intraradical fungal structures (white
947 dashed line). Scale bars = 50 μm.
948 Terminal and central sections from 1 cm-long sub-hyphopodial ROC segments were excised and
949 used for ploidy analysis through flow cytometry (c, d). Results demonstrated that 2.02% of nuclei in
950 terminal sections were endoreduplicated (8C and higher ploidy classes), while this population
951 increased to 3.43% in central sections. Chi-Square analysis identified a significant difference
952 between percentages of endoreduplicated nuclei (> 8C) in terminal and central root sections ($P <$
953 0.01). Histograms report average values from three independent experiments; error bars represent
954 standard deviations.
955
956 **Fig. 5. Average nuclear areas and volumes in uninoculated and inoculated *dmi2-2* and *dmi3-1***
957 **ROCs.** Histograms report average areas (a, b) and volumes (c, d) of DAPI-stained nuclei in
958 uninoculated and inoculated ROC segments from *dmi2-2* (a, c) and *dmi3-1* (b, d) *M. truncatula*
959 mutants. No statistically significant difference was observed in inoculated segments of either
960 mutant line (independent sample median tests; $P > 0.05$). Bars represent standard errors. *G. m*. =
961 *Gigaspora margarita*.
962
963 **Fig. 6. Analysis of ploidy in uninoculated and inoculated segments of *dmi2-2* and *dmi3-1 M.***
964 ***truncatula* ROCs.** Around 99% of nuclei in both uninoculated (a) and inoculated (sub-hyphopodial)
965 *dmi2-2* ROC segments (b) displayed 2C and 4C ploidy levels, with a comparably small percentage
966 (around 1%) of endoreduplicated nuclei (8C to 128C). The same scenario was observed in *dmi3-1*
967 mutants (c, d). Chi-Square analysis confirmed no significant differences between percentages of
968 endoreduplicated nuclei (> 8C) in uninoculated and inoculated roots of mutant lines ($P > 0.05$).
969 Histograms report average values from two independent experiments; error bars represent
970 standard deviations. *G. m*. = *Gigaspora margarita*.
971

Fig. 7. Regulation of endoreduplication markers and S-phase related genes in wild-type, *dmi2-2* and *dmi3-1* mutant ROCS at 48-60 hours after hyphopodium development.

The scheme in (a), modified from Kalve *et al*. (2014), represents the regulatory machinery of the G2-M switch, controlling endocycle activation. Low levels of G2-M cyclins CYCA2 and CYCB1, and the consequent triggering of endoreduplication, are obtained through both transcriptional repression and proteolysis. *CYCA2* expression is inhibited by ILP1 (Increased level of polyploidy 1), while *CYCB1* is repressed by MYB3R transcription factors. Proteolytic degradation of both cyclins is activated by APC/C (Anaphase Promoting Complex/Cyclosome), an E3 ubiquitin ligase, following its activation by the CCS52A (Cell Cycle Switch 52A) transcription factor. Endocycle inhibition (or entry into the M phase) is mediated by other transcription factors such as UVI4 (ULTRAVIOLET-B-INSENSITIVE 4) and DEL1 (DP-E2F-like transcription factor E2Fe-DEL1) that inhibit APC/C. By contrast, endocycle onset has been associated with the modulation of APC/C complex through down-regulation of *E2F-DEL1* and *UVI4* induced by DELLA proteins (Claey *et al*., 2012). The CSSP-induced gibberellin repressor protein DELLAs are transcription regulators that have recently been involved in regulation of arbuscule development and cell cycle (Floss *et al*., 2013; Takeda *et al*., 2015). Endocycle-associated rounds of DNA replication require the expression of histones (H4, H3, H2A and H2B) and DNA topoisomerase VI (*TOPO-VI*). Question marks indicate partially unexplored regulatory pathways. Genes of interest for this research are highlighted in red and their expression levels in sub-hyphopodial compared to uninoculated ROC segments are reported in panel (b). In detail, transcript levels were compared in uninoculated (white histograms) and inoculated (sub-hyphopodial) root segments (grey histograms) on wild-type, *dmi2-2* and *dmi3-1* ROCs. *APC/C subunit 2* and *CCS52A* transcripts were significantly upregulated in inoculated wild-type compared to controls, while no significant differences were observed in *dmi2-2* and *dmi3-1* mutants, where fungal penetration is arrested at hyphopodium development. A comparable regulation was observed in wild-type for A (*TOPO-VI A*) and B (*TOPO-VI B*) subunits of DNA Topoisomerase VI. By contrast, a differential regulation was recorded in mutants: *TOPO-VI A* was significantly down-regulated in *dmi2-2* and upregulated in *dmi3-1* inoculated roots, while no change was observed in *Topo-VI B* expression. *Hist-H4* expression was significantly upregulated only in inoculated wild-type, while the transcript level of *E2F-DEL1* remained unchanged in all samples. Fold changes (relative expression levels) are normalized to the corresponding controls. Histograms represent the mean of four biological replicates. Error bars indicate standard errors. Asterisks indicate statistically significant differences; T-test p value < 0.03. *G. m*. = *Gigaspora margarita*.

Fig. 8. Maps of putative ploidy in uninoculated and mycorrhizal *M. truncatula* ROCs. (a) All nuclear areas manually measured in 375x375x45µm z-stack projections from *M. truncatula* uninoculated (25 images, 3600 nuclei) and mycorrhizal (25 images, 3850 nuclei) ROC segments were clustered according to Sturges' rule into 15 μm^2 wide classes. Five and eight classes were identified in uninoculated and mycorrhizal sections, respectively, corresponding to ploidy classes identified by flow cytometry. Size limits and average area (μm^2) ± standard deviation are presented for each class. Nuclear classes were used to assemble the composite images such as those shown in (b, c): nuclear sizes were mapped using tags of the same color as the class background in table (a). In uninoculated roots (b), red tagged nuclei are mainly localized in the epidermis, while cortical cells contain both red and orange nuclei. When visible, central cylinder cells (which are never colonized by AM fungi) also contained a majority of red tagged nuclei. AM colonization (c) is associated with the appearance of yellow circles (class VI, VII and VIII) in arbusculated and neighboring cortical cells. Fungal structures are outlined in white. Scale bar = 50 µm.

15 maps of nuclear areas from uninoculated and mycorrhizal ROC segments were then used to analyze the distribution of nuclear classes in epidermal and cortical tissues, as reported in (d). The majority of epidermal nuclei belonged to class I, with a small percentage of class II nuclei in both uninoculated and mycorrhizal segments. By contrast, a major change was observed in the cortex upon AM colonization: while class I and II nuclei showed a small decrease (from 57.3% to 55.8%), the percentage of class III, IV and V nuclei increased from 13.4% in uninoculated to 18.5% in mycorrhizal samples, with the addition of 0.8% nuclei in the top three classes (VI, VII and VIII) that were never recorded in uninoculated roots. *G. m*. = *Gigaspora margarita*.

Fig. 9. Average nuclear area in different cell types from uninoculated and sub-hyphopodial ROC segments of wild-type, *dmi2-2* and *dmi3-1 M. truncatula*. For a more detailed representation of nuclear changes in wild-type mycorrhizal roots, we discriminated epidermal (E), cortical uncolonized (C), arbusculated (A) and neighboring (N) cells. Quantitative analysis was done on a dataset of 15 z-stacks for each condition (three genotypes, two treatments) and a total of 1175 and 1505 nuclei for wild-type (uninoculated and inoculated, respectively); 1145 and 1607 nuclei for *dmi2-2*; 1562 and 1175 nuclei for *dmi3-1*. The graph shows a significant increase in average nuclear size of arbusculated and uncolonized neighboring cells in wild-type roots, whereas no significant change is observed in either mutant upon AM inoculation. Different letters indicate statistically significant

differences; T-test *p* value < 0.001. Error bars represent standard deviations. *G. m*. = *Gigaspora margarita*.

Figure S1. Frequency distribution of nuclear areas and volumes in control and mycorrhizal roots of *M. truncatula*. Measures of nuclear areas (a) and volumes (b) as calculated by image analysis of DAPI-stained root sections show that wider ranges of frequency distribution are found in mycorrhizal (grey plots) compared to uninoculated root segments (white plots), with a statistically significant difference (Kruskal-Wallis test, $P < 0.01$). In more detail, nuclear areas in mycorrhizal sections ranged from 15 to 111 μm^2, compared to 15 to 43 μm^2 in uninoculated controls (a). Similarly, nuclear volumes (b) extended between 20 and 205 μm^3, compared to a range of 20 to 119 μm^3 in controls. *G. m*. = *Gigaspora margarita*.

Figure S2. **Frequency distribution of nuclear volumes in uninoculated and inoculated ROCs of wild-type, *dmi2-2* and *dmi3-1 M. truncatula*.** Measures of nuclear volumes as calculated by image analysis of DAPI-stained root sections collected 48-60 hours after hyphopodium formation show that a wider range of frequency distributions was recorded in mycorrhizal (grey plots) compared to uninoculated (white plots) wild-type ROCs (a): nuclear areas in mycorrhizal sections ranged from 20 to 220 μm^3, compared to 20 - 119 μm^3 in controls (a significant difference according to Kruskal-Wallis test, $P < 0.01$). By contrast, comparable frequency distributions (Kruskal-Wallis test at $P > 0.05$) were recorded for uninoculated (19-145 μm^3) and inoculated (19-147 μm^3) *dmi2-2* mutant ROCs, and the same observation was made in the *dmi3-1* mutant (19-136 μm^3 for controls and 19-151 μm^3 for sub-hyphopodial segments). *G. m*. = *Gigaspora margarita*.

Figure S3. Gene expression analysis of mycorrhizal markers *MtBCBP* and *MtPUB1*, and the alternative endocycle regulator *MtILP1* in ROC segments sampled 48-60 hours after hyphopodium development. The statistically significant upregulation of two acknowledged AM markers (a,b), *Blue copper-binding protein* (*MtBCBP*) and *E3 ubiquitin ligase* (*MtPUB1*), confirmed AM establishment in wild-type sub-hyphopodial root segments compared to uninoculated controls. *MtBCBP* and *MtPUB1* expression did not change in inoculated ROCs from *dmi2-2* and *dmi3-1* mutants compared to their respective controls, confirming the block of intraradical fungal development and symbiosis establishment in both mutants. The expression of *Increased level of polyploidy 1* (*MtILP1*), a key member of an alternative regulatory pathway for endocycle activation (c), did not change

significantly in mycorrhizal compared to uninoculated wild-type ROCs. Conversely, *MtILP1* expression increased significantly in inoculated segments from *dmi2-2* and *dmi3-1* mutants compared to their uninoculated controls. Relative gene expression levels (fold change) are normalized to the uninoculated controls. Asterisks indicate statistically significant differences; T-test *p* value < 0.03. Error bars represent standard errors. *G. m*. = *Gigaspora margarita*.

Figure S4. Correlation between nuclear classes (y-axis) and ploidy levels (x-axis). A significant positive logarithmic correlation ($R^2 > 0.99$) was demonstrated between the average area of each nuclear class and ploidy levels in *M. truncatula* wild-type uninoculated (a) and mycorrhizal (b) ROC segments; *dmi2-2* mutant uninoculated (c) and inoculated sub-hyphopodial segments (d); *dmi3-1* mutant uninoculated (e) and sub-hyphopodial (f) segments. Fisher's test *p* value < 0.05. *G. m*. = *Gigaspora margarita*.

Figure S5. Maximum brightness projections of confocal z-stacks from DAPI-stained wild-type, *dmi2-2* and *dmi3-1* ROC segments. Panels show representative images from the data set of 375x375x45µm z stacks that were used for image analysis to measure nuclear areas and volumes and assemble composite images such as those shown in Fig. 8 and Fig. S8. Fungal hyphae (hy), arbuscules (ar) and hyphopodia (hp) are recognizable in inoculated samples (b, d, f) by their clusters of small nuclei and were outlined in a white dashed line. Scale bars = 50 µm. *G. m*. = *Gigaspora margarita*.

Figure S6. Increase in nuclear areas throughout root colonization. The figure presents a collection of representative z-stack projections of progressive steps in wild-type *M. truncatula* ROC colonization by *G. margarita*. Numbers indicate the area of each nucleus in μm^2. Panel (a) shows a *G. margarita* hyphopodium (hp) contacting the root epidermis. The hyphopodium is recognizable as an expansion of the extraradical hypha (dashed outline) containing a cluster of small nuclei. All epidermal nuclei (including the nucleus of the contacted epidermal cell that has moved to the contact site - a hallmark of early prepenetration responses) belong to size class I (red, 15-30 μm^2), as defined by Sturges' rule, while cortical cell nuclei belong to class I and class II (red, 15-45 μm^2). An Intraradical hypha (hy) growing between cortical cells is shown in (b). Several neighboring cells display class III nuclei (orange, 45-60 μm^2); in addition, couples of short cells (yellow dashed outline) containing class II and III nuclei are found next to the intercellular hypha, suggesting the occurrence

of ectopic cell division (Russo *et al*., 2019). A global view of an early infection unit spreading across different root tissues is shown in (c): a hyphopodium (hp) is visible on the root surface from which intraradical hyphae (hy) extend to the inner cortex, where arbuscules have not yet formed. Several cells in the proximity of intraradical hyphae display class III, IV and V nuclei (orange, 45-90 μm^2). Two couples of short cortical cells (yellow outline) with class III nuclei are localized in the proximity of the hyphae. A single arbuscule has developed from hyphae colonizing the inner cortex in (d). The arbusculated cell has a class IV nucleus (orange, 60-75 μm^2) as well as a few other cells in the vicinity of the hyphae, while others contain class III nuclei (orange). More distant cells, by contrast, contain class I and II nuclei (in red). A couple of split cells (yellow outline) is found next to a hypha. Panel (e) shows another infection unit where a single arbuscule is visible. Colonized, and a few of the surrounding, cells display enlarged nuclei, with sizes reaching class V (orange, 75-90 μm^2). A more advanced infection unit is shown in (f), including several arbusculated cells with class III, IV and V nuclei (orange). Interestingly, a couple of split cells (yellow outline) has been colonized by two arbuscules. Panel (g) shows a mature infection unit, where all arbusculated cells have class III, IV, V and VI nuclei (orange; yellow, 90-105). Bars = 50 µm.

Figure S7. Maps of putative ploidy in uninoculated and inoculated ROC segments from *dmi2-2* and *dmi3-1* mutants. (a) All nuclear areas manually measured in 375x375x45µm z-stack projections from uninoculated and inoculated ROC segments were grouped by applying Sturges' rule into 13 μm^2 wide classes. 25 images were analysed for each condition, and 2800 and 3550 nuclei were measured for *dmi2-2* uninoculated and inoculated segments respectively; 3230 and 3500 nuclei for *dmi3-1*. Size limits and average area (μm^2) ± standard deviation are presented for each class. Seven classes were identified in uninoculated and inoculated samples from both mutants - corresponding to ploidy classes identified by flow cytometry - and used to assemble composite images as previously described for the wild-type (Fig. 8). Two representative maps of uninoculated (b, d) and inoculated (c, e) ROC segments are presented for *dmi2-2* (b, c) and *dmi3-1* (d, e). Comparable distributions of nuclear classes can be observed in inoculated and uninoculated ROCs of both mutants. In more detail, red tagged nuclei are present in epidermal, cortical and central cylinder cells; orange nuclei concentrate in cortical cells, with a few in the central cylinder; a few yellow nuclei are occasionally observed in the central cylinder. These observations demonstrate the lack of nuclear changes in the absence of intraradical fungal colonization. The presence of larger nuclei in the central cylinder was

not recorded in the wild-type and could be a feature of *dmi2-2* and *dmi3-1* mutant phenotype. Bars = 50 µm. *G. m*. = *Gigaspora margarita*.

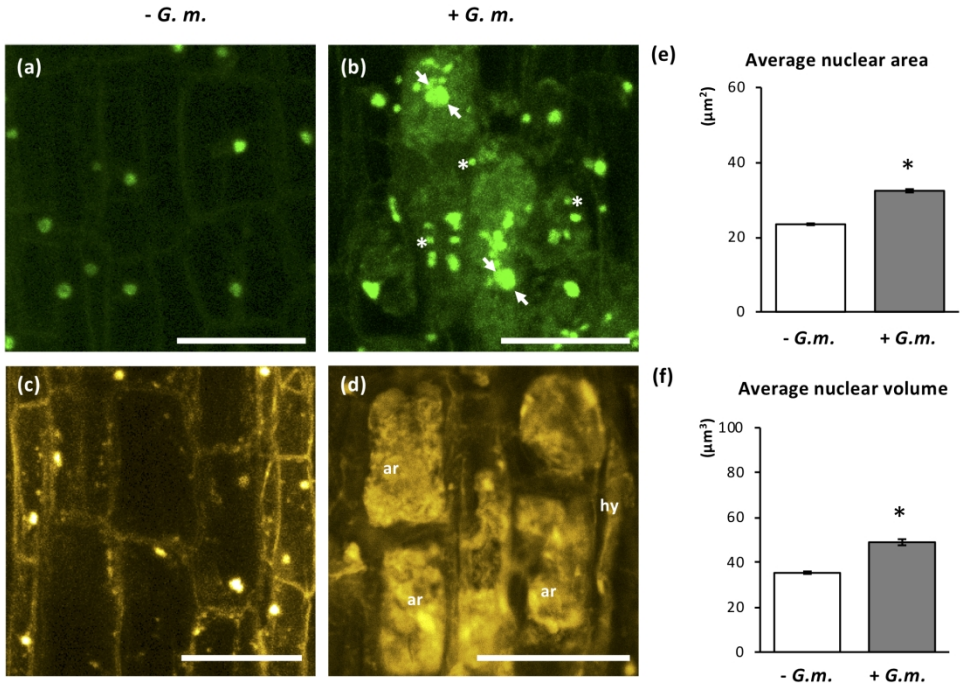

Fig. 1. Analysis of nuclear size in uninoculated and mycorrhizal roots of M. truncatula. Representative confocal images (z-stack projections) of longitudinal root sections from pot grown M. truncatula stained with DAPI to visualize nuclear morphology (a,b) and acid fuchsin (c,d) to highlight intraradical hyphae (hy) and arbuscules (ar). DAPI staining revealed an apparent increase in nuclear size (b, white arrows) for all colonized cortical cells from mycorrhizal roots. After the comparison with fuchsin-stained samples, intraradical fungal structures are easily recognizable in DAPI images by their numerous small nuclei (asterisks) and a diffuse background fluorescence. Scale bars = 50 □m.
Histograms in (e,f) report average nuclear areas (e) and volumes (f) as estimated through image analysis of 2052 and 2222 DAPI-stained nuclei from 20 uninoculated and 20 mycorrhizal root segments respectively. Colonization of cortical cells produced a significant increase in both nuclear areas and volumes. Bars represent standard errors; asterisks indicate statistically significant differences based on independent sample median tests for data with non-normal distribution ($P < 0.01$). G. m. = Gigaspora margarita.

192x140mm (300 x 300 DPI)

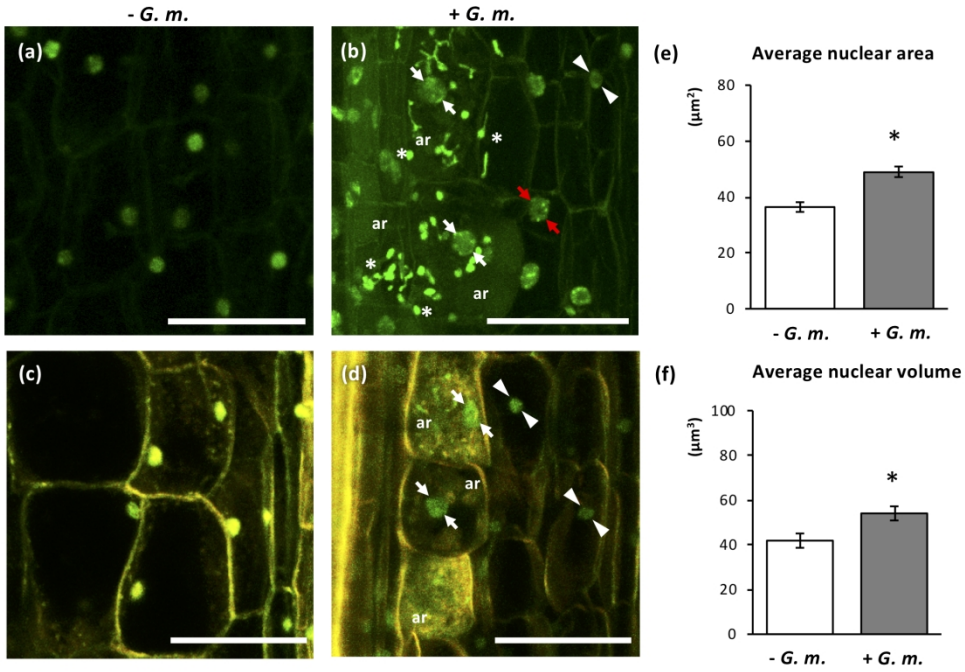

Fig. 2. Analysis of nuclear size in uninoculated and mycorrhizal M. truncatula ROCs. Representative images of longitudinal sections stained with DAPI (green, a, b) and SR2200 (gold, c, d) show nuclear and cell wall morphology in uninoculated (a, c) and mycorrhizal (b, d) segments of root organ cultures (ROCs). Large nuclei were found in arbusculated cells (white arrows) and some of the neighboring cortical cells (red arrows), compared to the smaller nuclei of distant cortical cells (white arrowheads), which were comparable in size to those observed in uninoculated roots (a, c). Small-sized fungal nuclei are evident in hyphae and arbuscules (asterisks). DAPI-SR2200 counter-staining (c, d) provided a clearer labeling of plant and fungal (ar) walls, confirming the increase in nuclear size (white arrows) of arbusculated versus uncolonized cortical cells (arrowheads). Scale bars = 50 □m.

Histograms in (e) report average areas of 3600 and 3850 DAPI-stained nuclei from 25 uninoculated and 25 mycorrhizal root segments respectively. Histograms in (f) represent average calculated volumes of 2000 and 2449 nuclei from the same respective samples. Both nuclear areas and volumes significantly increased in mycorrhizal compared to uninoculated ROCs. Bars represent standard errors; asterisks indicate statistically significant differences based on independent sample median tests ($P < 0.01$). G. m. = Gigaspora margarita.

193x137mm (300 x 300 DPI)

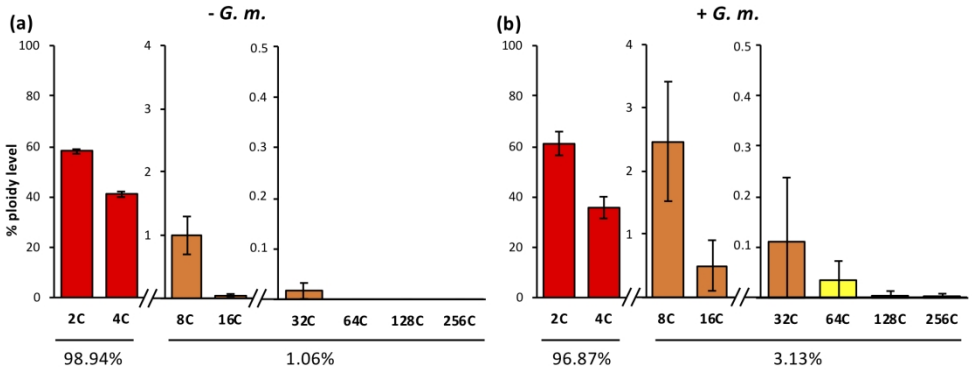

Fig. 3. Analysis of ploidy by flow cytometry in uninoculated and mycorrhizal M. truncatula ROC segments. The majority of nuclei in uninoculated segments (a) consisted of 2C and 4C nuclei (98.94%), while endoreduplicated nuclei (8C, 16C and 32C) represented 1.06% of extracted nuclei. By contrast, a three-fold increase in the percentage of endoreduplicated nuclei (3.13%) and the appearance of higher ploidy classes (64C, 128C and 256C) was recorded in mycorrhizal (sub-hyphopodial) segments. Chi-Square analysis identified a significant difference between percentages of endoreduplicated nuclei (above 8C) in uninoculated and mycorrhizal root segments ($P < 0.01$). Histograms report average values from three independent experiments; error bars represent standard deviations. G. m. = Gigaspora margarita.

204x88mm (300 x 300 DPI)

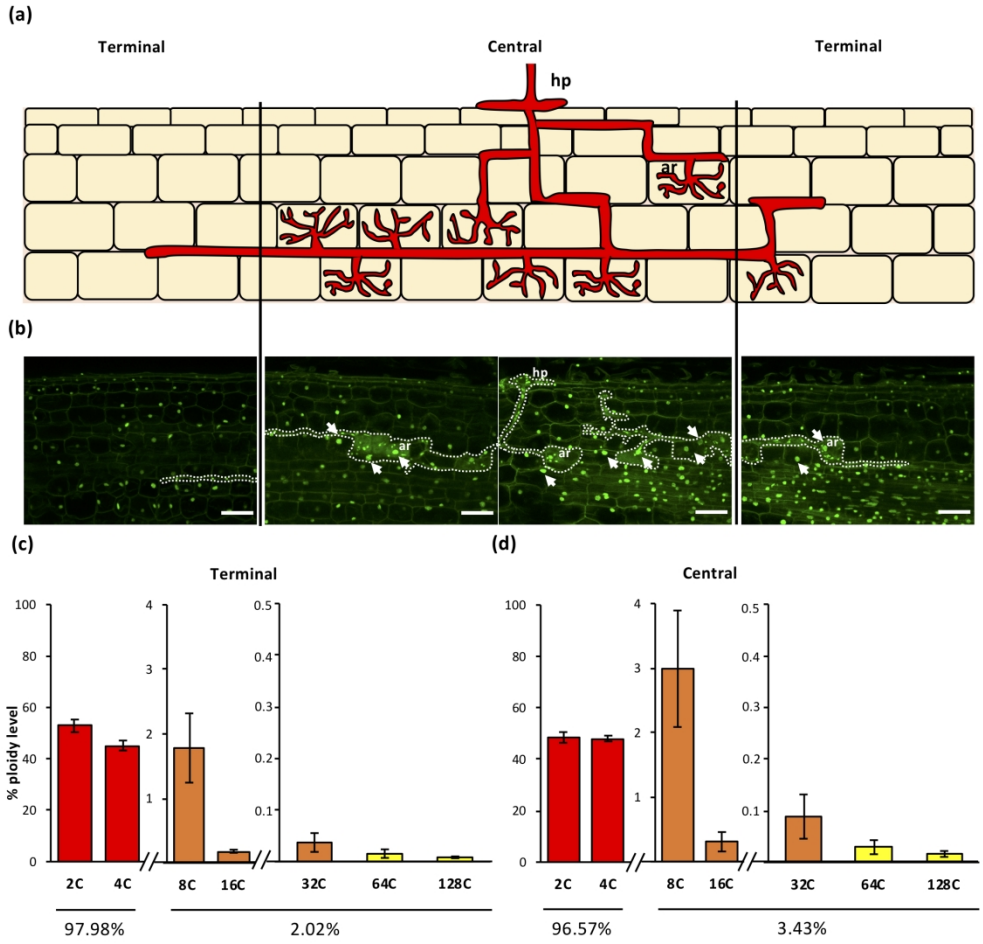

Fig. 4. Analysis of ploidy in central versus terminal zones of sub-hyphopodial M. truncatula ROC segments. The scheme in (a) represents a typical infection unit in 48-60 h old sub-hyphopodial segments of M. truncatula, with a patch of hyphae and arbuscules (ar) in the central zone, directly underneath the hyphopodium (hp), and very few intraradical fungal structures in either terminal end of the segment. Panels in (b) display corresponding confocal images from a DAPI-stained ROC segment. Larger nuclei (arrows) were more abundant in the central zone than in terminal ends, and characterized cells that were either colonized or adjacent to the intraradical fungal structures (white dashed line). Scale bars = 50 ☐m. Terminal and central sections from 1 cm-long sub-hyphopodial ROC segments were excised and used for ploidy analysis through flow cytometry (c, d). Results demonstrated that 2.02% of nuclei in terminal sections were endoreduplicated (8C and higher ploidy classes), while this population increased to 3.43% in central sections. Chi-Square analysis identified a significant difference between percentages of endoreduplicated nuclei (> 8C) in terminal and central root sections ($P < 0.01$). Histograms report average values from three independent experiments; error bars represent standard deviations.

200x193mm (300 x 300 DPI)

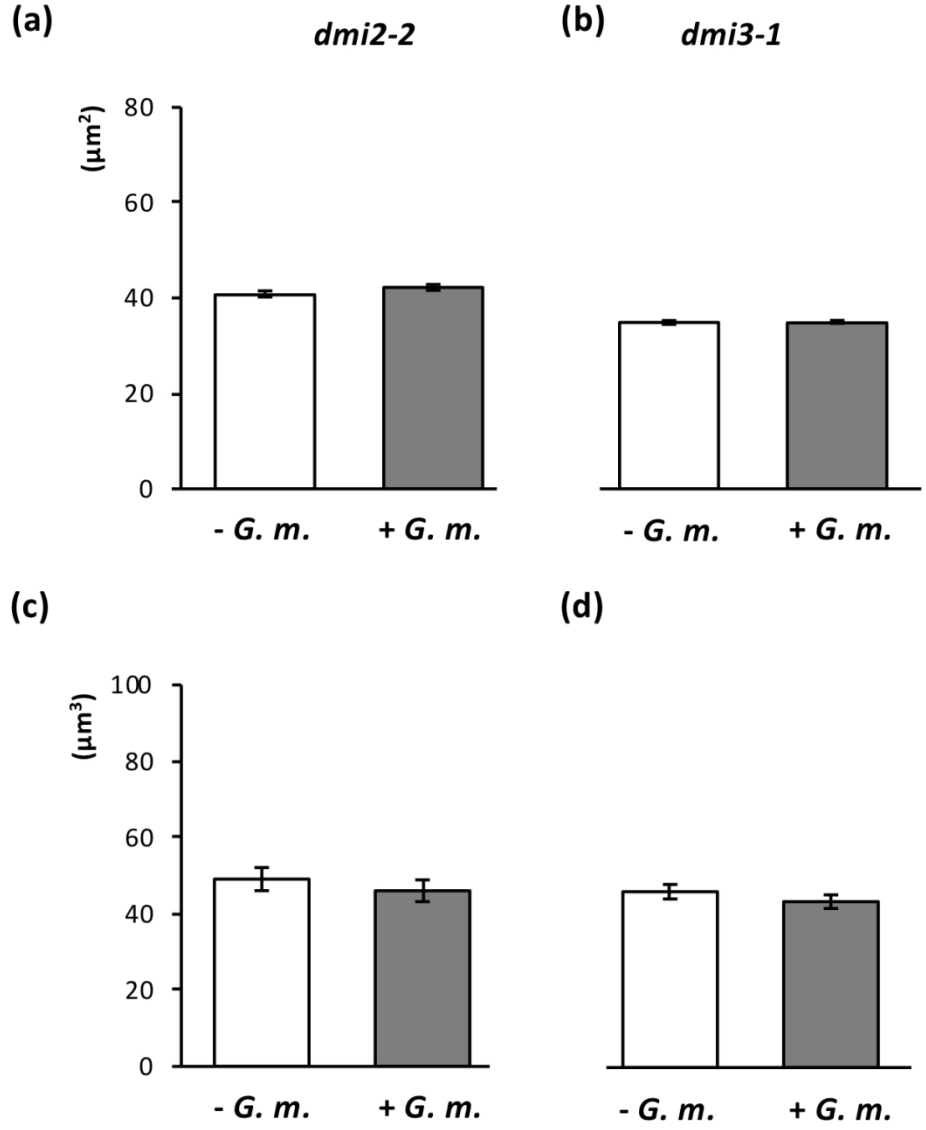

Fig. 5. Average nuclear areas and volumes in uninoculated and inoculated dmi2-2 and dmi3-1 ROCs. Histograms report average areas (a, b) and volumes (c, d) of DAPI-stained nuclei in uninoculated and inoculated ROC segments from dmi2-2 (a, c) and dmi3-1 (b, d) M. truncatula mutants. No statistically significant difference was observed in inoculated segments of either mutant line (independent sample median tests; $P > 0.05$). Bars represent standard errors. G. m. = Gigaspora margarita.

113x135mm (300 x 300 DPI)

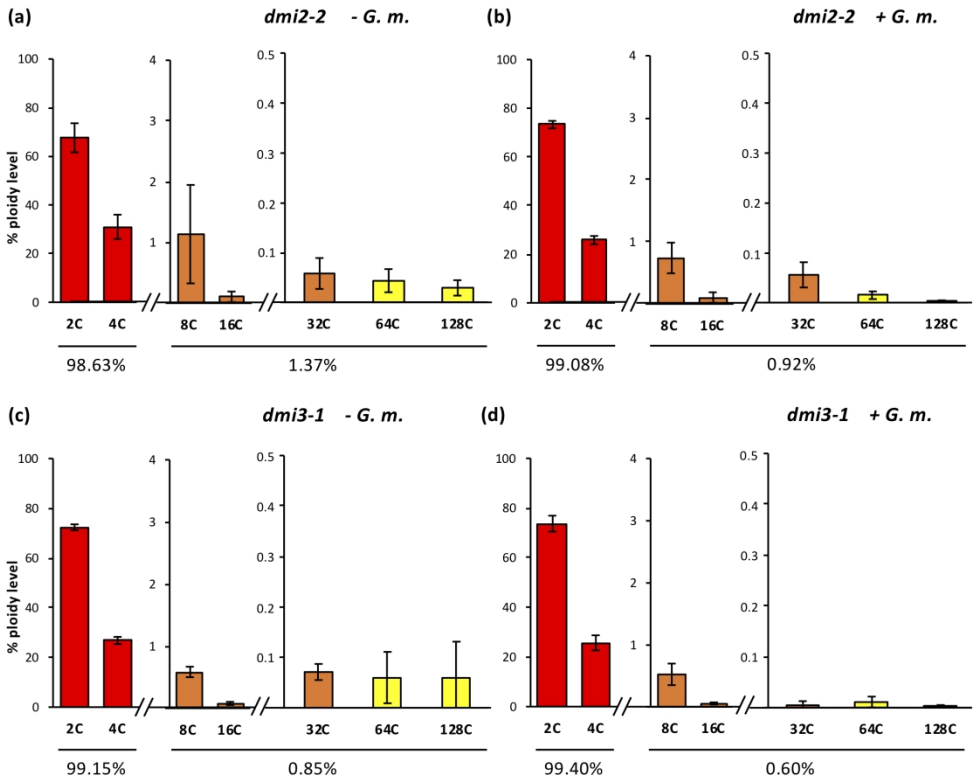

Fig. 6. Analysis of ploidy in uninoculated and inoculated segments of dmi2-2 and dmi3-1 M. truncatula ROCs. Around 99% of nuclei in both uninoculated (a) and inoculated (sub-hyphopodial) dmi2-2 ROC segments (b) displayed 2C and 4C ploidy levels, with a comparably small percentage (around 1%) of endoreduplicated nuclei (8C to 128C). The same scenario was observed in dmi3-1 mutants (c, d). Chi-Square analysis confirmed no significant differences between percentages of endoreduplicated nuclei (> 8C) in uninoculated and inoculated roots of mutant lines ($P > 0.05$). Histograms report average values from two independent experiments; error bars represent standard deviations. G. m. = Gigaspora margarita.

204x164mm (300 x 300 DPI)

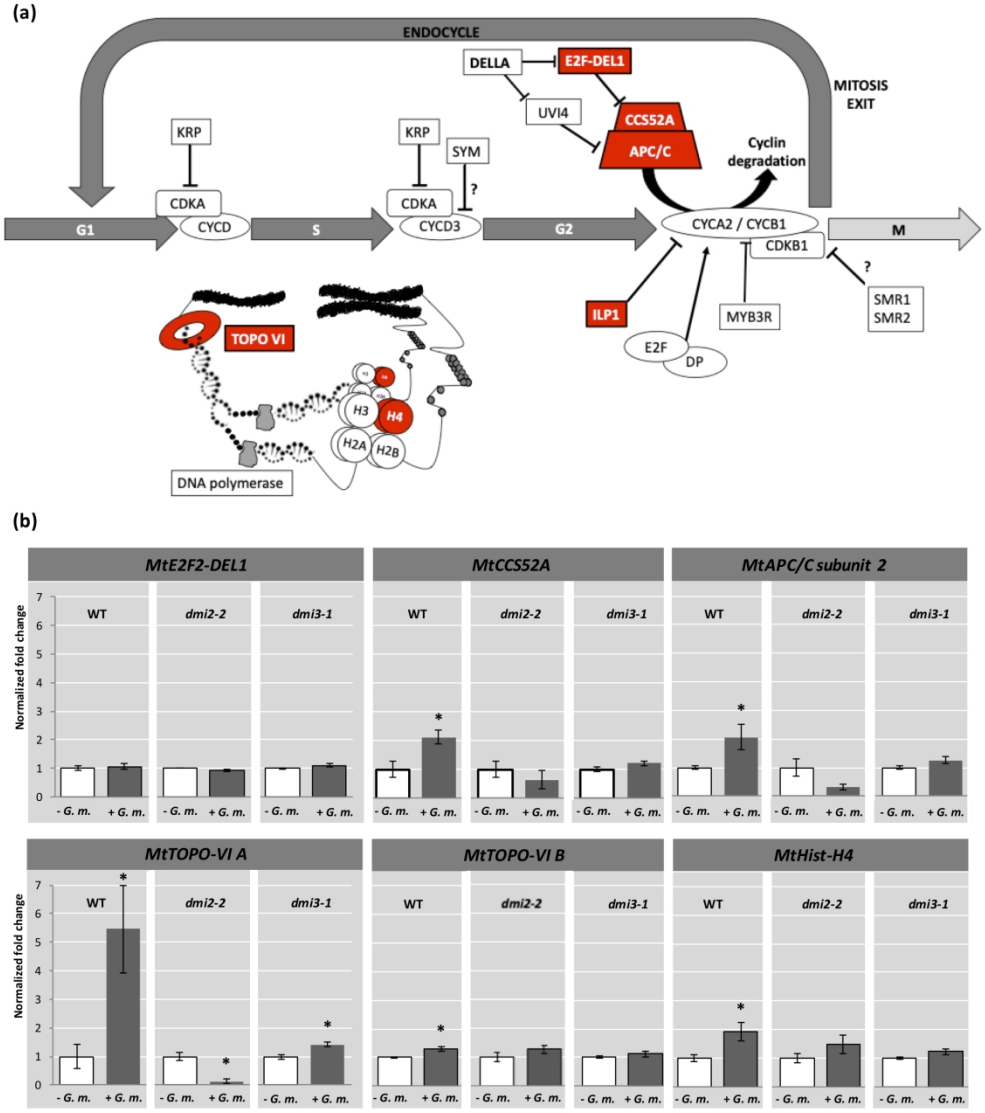

Fig. 7. Regulation of endoreduplication markers and S-phase related genes in wild-type, dmi2-2 and dmi3-1 mutant ROCS at 48-60 hours after hyphopodium development.

The scheme in (a), modified from Kalve et al. (2014), represents the regulatory machinery of the G2-M switch, controlling endocycle activation. Low levels of G2-M cyclins CYCA2 and CYCB1, and the consequent triggering of endoreduplication, are obtained through both transcriptional repression and proteolysis. CYCA2 expression is inhibited by ILP1 (Increased level of polyploidy 1), while CYCB1 is repressed by MYB3R transcription factors. Proteolytic degradation of both cyclins is activated by APC/C (Anaphase Promoting Complex/Cyclosome), an E3 ubiquitin ligase, following its activation by the CCS52A (Cell Cycle Switch 52A) transcription factor. Endocycle inhibition (or entry into the M phase) is mediated by other transcription factors such as UVI4 (ULTRAVIOLET-B-INSENSITIVE 4) and DEL1 (DP-E2F-like transcription factor E2Fe-DEL1) that inhibit APC/C. By contrast, endocycle is promoted by down-regulation of E2F-DEL1 and UVI4, induced by DELLA proteins (Claey et al., 2012). Endocycle-associated rounds of DNA replication require the expression of histones (H4, H3, H2A and H2B) and DNA topoisomerase VI (TOPO-VI). Question marks indicate partially unexplored regulatory pathways. Genes of interest for this research are highlighted in red and their expression levels in sub-hyphopodial compared to uninoculated ROC segments are reported in panel (b). In detail, transcript levels were compared in uninoculated (white histograms) and inoculated (sub-

hyphopodial) root segments (grey histograms) on wild-type, dmi2-2 and dmi3-1 ROCs. APC/C subunit 2 and CCS52A transcripts were significantly upregulated in inoculated wild-type compared to controls, while no significant differences were observed in dmi2-2 and dmi3-1 mutants, where fungal penetration is arrested at hyphopodium development. A comparable regulation was observed in wild-type for A (TOPO-VI A) and B (TOPO-VI B) subunits of DNA Topoisomerase VI. By contrast, a differential regulation was recorded in mutants: TOPO-VI A was significantly down-regulated in dmi2-2 and upregulated in dmi3-1 inoculated roots, while no change was observed in Topo-VI B expression. Hist-H4 expression was significantly upregulated only in inoculated wild-type, while the transcript level of E2F-DEL1 remained unchanged in all samples. Fold changes (relative expression levels) are normalized to the corresponding controls. Histograms represent the mean of four biological replicates. Error bars indicate standard errors. Asterisks indicate statistically significant differences; T-test p value < 0.03. G. m. = Gigaspora margarita.

201x228mm (300 x 300 DPI)

(a)

Classes of nuclear sizes

	I 15-30	II 30-45	III 45-60	IV 60-75	V 75-90	VI 90-105	VII 105-120	VIII 120-135
- G. m.	21.3 ± 5.0	36.0 ± 3.9	52.4 ± 4.8	65.3 ± 4.6	76.5 ± 2.9			
+ G. m.	22.2 ± 5.3	39.6 ± 3.9	51.9 ± 4.4	66.7 ± 3.9	82.2 ± 3.7	95.5 ± 3.1	114.9 ± 4.9	127 ± 0.0

(b)

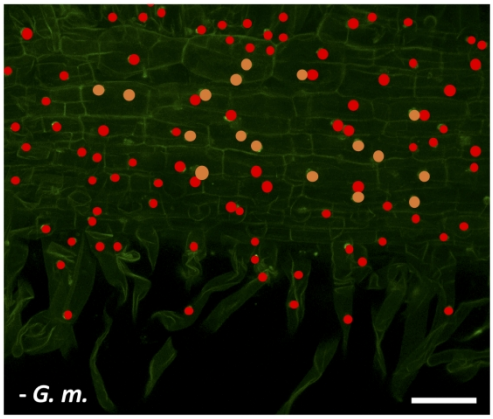

(c)

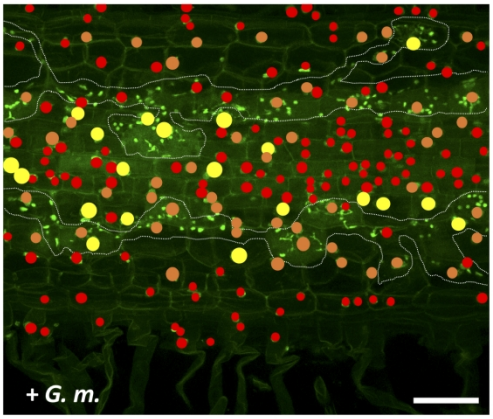

(d)

Percentage of nuclei for each class in root tissues

		I	II	III	IV	V	VI	VII	VIII
- G. m.	Epid	29.1%	0.3%						
	Cort	24.8%	32.5%	12.2%	1.0%	0.1%			
+ G. m.	Epid	24.3%	0.6%						
	Cort	20.6%	35.2%	13.0%	4.0%	1.5%	0.6%	0.1%	0.1%

Fig. 8. Maps of putative ploidy in uninoculated and mycorrhizal M. truncatula ROCs. (a) All nuclear areas manually measured in 375x375x45µm z-stack projections from M. truncatula uninoculated (25 images, 3600 nuclei) and mycorrhizal (25 images, 3850 nuclei) ROC segments were clustered according to Sturges' rule into 15 µm2 wide classes. Five and eight classes were identified in uninoculated and mycorrhizal sections, respectively, corresponding to ploidy classes identified by flow cytometry. Size limits and average area (µm2) ± standard deviation are presented for each class.

Nuclear classes were used to assemble the composite images such as those shown in (b, c): nuclear sizes were mapped using tags of the same color as the class background in table (a). In uninoculated roots (b), red tagged nuclei are mainly localized in the epidermis, while cortical cells contain both red and orange nuclei. When visible, central cylinder cells (which are never colonized by AM fungi) also contained a majority of red tagged nuclei. AM colonization (c) is associated with the appearance of yellow circles (class VI, VII and VIII) in arbusculated and neighboring cortical cells. Fungal structures are outlined in white. Scale bar = 50 µm.

15 maps of nuclear areas from uninoculated and mycorrhizal ROC segments were then used to analyze the distribution of nuclear classes in epidermal and cortical tissues, as reported in (d). The majority of epidermal nuclei belonged to class I, with a small percentage of class II nuclei in both uninoculated and mycorrhizal segments. By contrast, a major change was observed in the cortex upon AM colonization: while class I and II nuclei showed a small decrease (from 57.3% to 55.8%), the percentage of class III, IV and V nuclei

increased from 13.4% in uninoculated to 18.5% in mycorrhizal samples, with the addition of 0.8% nuclei in the top three classes (VI, VII and VIII) that were never recorded in uninoculated roots. G. m. = Gigaspora margarita.

200x217mm (300 x 300 DPI)

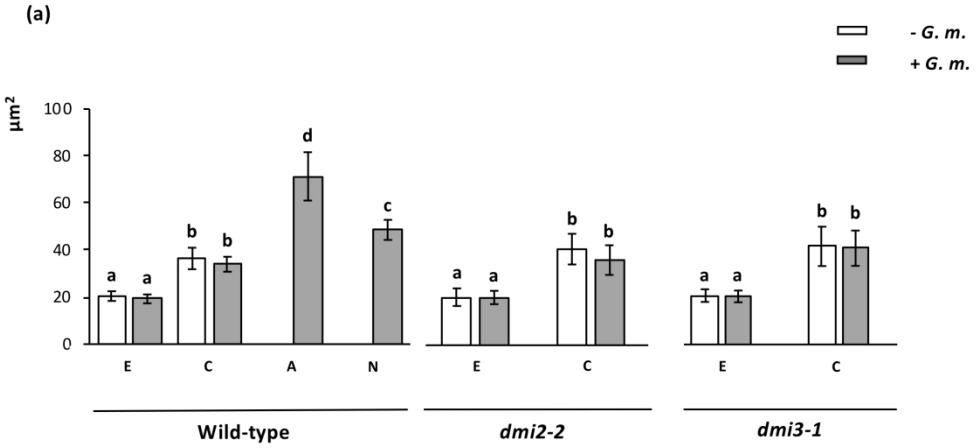

Fig. 9. Average nuclear area in different cell types from uninoculated and sub-hyphopodial ROC segments of wild-type, dmi2-2 and dmi3-1 M. truncatula. For a more detailed representation of nuclear changes in wild-type mycorrhizal roots, we discriminated epidermal (E), cortical uncolonized (C), arbusculated (A) and neighboring (N) cells. Quantitative analysis was done on a dataset of 15 z-stacks for each condition (three genotypes, two treatments) and a total of 1175 and 1505 nuclei for wild-type (uninoculated and inoculated, respectively); 1145 and 1607 nuclei for dmi2-2; 1562 and 1175 nuclei for dmi3-1. The graph shows a significant increase in average nuclear size of arbusculated and uncolonized neighboring cells in wild-type roots, whereas no significant change is observed in either mutant upon AM inoculation. Different letters indicate statistically significant differences; T-test p value < 0.001. Error bars represent standard deviations. G. m. = Gigaspora margarita.

195x94mm (300 x 300 DPI)